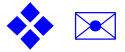


# Estimating the contribution of early and late noise in vision from psychophysical data

**Jesús Malo**

Image Processing Lab, Parc Científic  
Universitat de València, Spain



**José Juan Esteve-Taboada**

Dept. Optics, School of Physics  
Universitat de València, Spain



**Guillermo Aguilar**

Computational Psychology  
Technische Universität Berlin, Germany



**Marianne Maertens**

Computational Psychology  
Technische Universität Berlin, Germany



**Felix Wichmann**

Neural Information Processing Group  
University of Tübingen, Germany



In many psychophysical detection and discrimination tasks human performance is thought to be limited by internal or inner noise when neuronal activity is converted into an overt behavioural response. It is unclear, however, to what extent the behaviourally limiting inner noise arises from *early* noise in the photoreceptors and the retina, or from *late* noise in cortex at or immediately prior to the decision stage. Presumably, the behaviourally limiting *inner noise* is a non-trivial combination of both *early* and *late* noises. Here we propose a method to quantify the contributions of early and late noise purely from psychophysical data. Our analysis generalizes classical results for linear systems (Burgess and Colborne, 1988) by combining the theory of noise propagation through a nonlinear network (Ahumada, 1987) with the expressions to obtain the perceptual metric along the nonlinear network (Malo and Simoncelli, 2006; Laparra et al., 2010). We show that from threshold-only data the relative contribution of early and late noise can only be determined if the experiments include substantial *external* noise in some of the stimuli used during experiments. If experimenters collected full psychometric functions, however, then early and late noise sources can be quantified even in the absence of external noise. Our psychophysical estimate of the magnitude of the early noise—assuming a standard cascade of linear and nonlinear model stages—is substantially lower than the noise in cone photocurrents computed via an accurate model of retinal physiology (Brainard and Wandell, 2020, ISETBIO). This is consistent with the idea that one of the fundamental tasks of early vision is to reduce the comparatively large retinal noise.

Keywords: Early noise, late noise, external noise, spatial vision, pattern discrimination, linear-nonlinear models, information transmission.

## 1. Introduction

Relating the physical properties of a distal stimulus to its perception is the foundational question in psychophysics. One common and important observation is that perception is typically variable even if an unchanging physical stimulus is repeatedly presented—at least if the stimulus is presented such that it is neither trivially easy nor impossible to be perceived (neither “at ceiling” nor “at the floor”). At the latest since the advent of signal detection theory (SDT) in the 1950’s the source of this behavioural variability is conceptualised and modelled as arising from internal noise on a putative decision- or evidence-axis (Tanner and Swets, 1954; Swets, 1961; Green and Swets, 1988). In this widely accepted view perceptual detection and discrimination behaviour depends on the strength of the internal response to a stimulus relative to the internal variability (“signal and noise”).

From a neurophysiological standpoint noise sources in sensory systems are multiple and arise at every stage within the system. In the visual system neuronal variability—noise—can be observed from photon detection in the photoreceptors to the variability of responses of all neurons along the visual pathways. The effect of the different neurophysiologically measured noise sources on explicit behaviour in psychophysics is unclear, however.

Thus, and despite the *neuroscientific* identification of many noise sources, perceptual models of human visual behaviour commonly refer to all noise sources together as internal or inner noise (Burgess and Colborne, 1988). Typically the internal noise is modelled as a single late noise source, i.e. the only noise source in typical models is added as decision noise after all processing stages in the model. Discussion of noise in psychophysical models is predominantly limited to the type of late noise, i.e. whether its variance is fixed or varies with signal strength (e.g. fixed variance Gaussian versus Gaussian noise with signal-dependent variance or Poisson noise, see Wichmann, 1999; Georgeson and Meese, 2006a). A discussion of the number of noise sources and their position within the (nonlinear) processing stages is comparatively rare, however (Pelli, 1991; Pelli and Farell, 1999).

Pragmatically this may appear understandable given that performance or discrimination ability of a model is determined by the variability of the responses at the inner representation of the model, i.e. after the patterns have propagated through—and are changed by—the system. However, to obtain more detailed and accurate mechanistic models of the visual system the individual contributions to the the internal or inner noise may be of interest: How much of it results from, first, the propagation of the uncertainty in the input signal (if there is *external noise*), second from the *early noise* up to the inner, behaviourally relevant representation plus, third, the noise added at this final stage (*late noise*).

We believe there are at least two reasons why the question of the number and type of noise sources in behavioural models of perception is rarely explored and thus still wide open:

1. Psychophysically, all we can measure is the probability of correct detection or discrimination as a function of stimulus intensity or stimulus differences—but both nonlinearities and noise co-determine performance, and strong statements about the type of noise can only be made for a fixed nonlinear transformation (and vice versa).
2. Inclusion of early noise sources complicates matters considerably: early noise, like the stimulus itself, will be nonlinearly transformed through the system, typically resulting in noise for which no closed-form expression exists—the behaviour of such a model would thus require (extensive) numerical simulations, and fitting such a model to psychophysical data is likely to be more difficult.

Here we propose a strategy to estimate the different components of internal noise—early and late—within the nonlinear processing cascade based on psychophysical data only (and a given, fixed, nonlinear processing model). To this end we combine the theory of noise propagation through a network (Ahumada, 1987) with the expressions to obtain the perceptual metric along the network (Malo, 1999; Malo and Simoncelli, 2006; Laparra et al., 2010).

## Outline

The structure of the paper is as follows: In section 2 we introduce our notation, a simple (linear-nonlinear) early vision model we use to illustrate our method, as well as the experimental data we use to estimate early and late noise parameters. In section 3 we describe the idea of propagating a stimulus perturbed by noise through a linear-nonlinear early vision model. We show how our method generalizes the classical result of [Burgess and Colborne \(1988\)](#), and discuss the key role of the *external* noise required in threshold-only experiments to be able to determine the relative magnitude of early and late noise sources *internal* to the visual system. In section 4 we show that we can estimate the early and late noise sources as well as their relative magnitude even without external noise if we have full psychometric functions and not only threshold estimates. In section 5 we compare physiological noise estimates in the retina with those obtained from our method using only psychophysical data. The discussion in section 6, finally, concludes our paper.

## 2. Notation, illustrative vision model and data

### 2.1 Notation

We assume a vision model  $S$ , transforming visual input—the vector  $\mathbf{x}$ —into a perceptual response, the vector  $\mathbf{y}$ ,

$$\begin{array}{ccc}
 & S & \\
 & \curvearrowright & \\
 \mathbf{x} + \mathbf{n}_\varepsilon + \mathbf{n}_e & & \mathbf{y} = S(\mathbf{x} + \mathbf{n}_\varepsilon + \mathbf{n}_e) + \mathbf{n}_l \\
 & & \mathbf{y} = S(\mathbf{x}) + \mathbf{n}_\mathcal{I}
 \end{array} \quad (1)$$

While we assume the transform  $S$  to be deterministic, the input to  $S$  is assumed to be corrupted by *early noise*  $\mathbf{n}_e$  that is added at the levels of the photoreceptors. We also assume that the output from  $S$  is corrupted by *late noise*  $\mathbf{n}_l$  which is introduced at the level of the perceptual representation or at the decision stage.

In addition, we consider an *external noise*  $\mathbf{n}_\varepsilon$  which can be added to the stimulus by the experimenter in order to probe the processing characteristics of the system under study. All of these noise sources, external, early intrinsic and late intrinsic, can be summarized into a single noise term *internal noise*,  $\mathbf{n}_\mathcal{I}$  which is added to the deterministic response of the system. The *internal noise*,  $\mathbf{n}_\mathcal{I}$  is the difference between the noisy response and the deterministic response to the stimulus,  $\mathbf{n}_\mathcal{I} = \mathbf{y} - S(\mathbf{x})$ . It is this internal noise,  $\mathbf{n}_\mathcal{I}$ , which effectively limits the performance of the observer in discriminating two similar stimuli  $\mathbf{x}_1$  and  $\mathbf{x}_2$  if the difference of system responses  $\Delta S = S(\mathbf{x}_2) - S(\mathbf{x}_1)$  is small relative to the internal noise:  $\mathbf{n}_\mathcal{I} \gg \Delta S$ .

### 2.2 Illustrative vision model

The vision model we adopt as the deterministic transform  $S$  is a standard early visual model composed of a linear stage—wavelet filters scaled in agreement with the contrast sensitivity function (CSF; [Robson \(1966\)](#))—followed by a point-wise nonlinearity  $m$ :

$$\begin{array}{ccccc}
 & & S & & \\
 & & \curvearrowright & & \\
 \mathbf{x} + \mathbf{n}_\varepsilon + \mathbf{n}_e & & \mathbf{w} & \mathbf{w}' & \mathbf{y} = S(\mathbf{x} + \mathbf{n}_\varepsilon + \mathbf{n}_e) + \mathbf{n}_l \\
 & \curvearrowright & \curvearrowright & \curvearrowright & \\
 W \equiv \text{wavelets} & \mathbb{D}_{CSF} & m(\mathbf{w}') \equiv \text{nonlinearity} & & 
 \end{array} \quad (2)$$

The input to the deterministic model  $S$  consists of the stimulus plus the external noise,  $\mathbf{x} + \mathbf{n}_\varepsilon$ , and the early (photoreceptor) noise  $\mathbf{n}_e$ , all expressed in units of  $cd/m^2$ . Following ([Brainard and Wandell, 2020](#); [Dayan and Abbott, 2005](#)) we assume that the early noise follows a simple Gaussian-Poisson distribution (see Eq. 17 in Appendix A for the expression of the signal-dependent covariance). The (psychophysical) scaling parameter (Fano factor,  $\beta_e$ ) of this distribution is unknown and its determination is one of the goals of our study.

The first step in the model  $S$  is to apply a set of local, oriented filters of different scales to the input (see, e.g., [Watson, 1987](#)). This linear transform is followed by a scale dependent weighting which simulates the effect of the CSF. We use a steerable wavelet transform ([Simoncelli et al., 1992](#)) for the linear filters and the method in ([Malo et al., 1997](#)) to get the optimal CSF weights in that domain—mainly because of mathematical beauty and computational simplicity. This linear stage can be summarized as the product of two matrices:  $\mathbf{w}' = \mathbb{D}_{\text{CSF}} \cdot W \cdot (\mathbf{x} + \mathbf{n}_\varepsilon + \mathbf{n}_e)$ , where  $W$  contains the wavelet receptive fields in rows and  $\mathbb{D}_{\text{CSF}}$  is a diagonal matrix with the weights that represent the CSF in the diagonal. In the final step we apply point-wise saturating functions to each coefficient of the linear transform ([Legge and Foley, 1980](#); [Legge, 1981](#)). Specifically,  $\mathbf{y} = m(\mathbf{w}') + \mathbf{n}_l = K \odot \text{sign}(\mathbf{w}') \odot |\mathbf{w}'|^\gamma + \mathbf{n}_l$ . Where  $\mathbf{a} \odot \mathbf{b}$  represents the element-wise product of vectors  $\mathbf{a}$  and  $\mathbf{b}$ , the exponent  $\gamma$  is applied element-wise to the absolute value of every component in  $\mathbf{w}'$ , and the original sign of the components is preserved through the  $\text{sign}(\cdot)$  function. Following ([Martinez et al., 2018](#)), we apply a correction at the origin to avoid singularities in the derivative, and following ([Martinez et al., 2019](#)) the constant  $K$  is chosen not to modify the relative magnitude of the sub-bands to preserve the effect of the CSF<sup>1</sup>.

Finally, we assume that the late noise  $\mathbf{n}_l$  also follows a Gaussian-Poisson distribution like the early noise (see covariance in Eq. 17 in Appendix A). Again, the goal of the proposed method is to obtain the Fano factor,  $\beta_l$ , of this distribution. Please note we assume level-dependent early and late noise sources for exposition in this work. However, using our methods we believe one should be able to investigate the role of level-independent late noise noise in models of spatial vision (see e.g. [Wichmann, 1999](#); [Kontsevich et al., 2002](#); [Georgeson and Meese, 2006b](#); [Schütt and Wichmann, 2017](#)), an issue we return to in the discussion.

The point of this somewhat simplistic model is not that it is a state-of-the-art model of early spatial vision: its elements—the wavelet transform and the CSF—are taken off-the-shelf and we chose reasonable values for its free parameters—the saturation exponent,  $\gamma$ , and the sub-band-dependent constant,  $K$ . For the present purpose we only need a *reasonably good* and *reasonably simple* model to illustrate the method of noise propagation to derive a perceptual metric: Reasonably good to be able to predict human data from detection and discrimination experiments with grating stimuli well, as shown below. Reasonably simple in order to have well behaved derivatives,  $\nabla S$  for computational reasons in the optimization. Note that in principle our method could of course be applied also to more sophisticated models of the transform  $S$ ; the estimation of the derivatives might then be more cumbersome, however, or may require numerical approximations.

## 2.3 Illustration in a toy example

Here we graphically illustrate the concepts and method in a toy scenario that deals with 2-pixel images. This minimal dimension allows the complete visualization of the noise sources, as shown in Fig.1. Despite its simplicity, this toy example has all the appropriate ingredients: First, a linear transform,  $W$ , which here is a rotation from the original pixel-luminance axes into the low-frequency/mean-luminance axis and the high-frequency/contrast axis<sup>2</sup>. Second, the CSF as a scalar weight in each component of the rotated domain (larger for the low frequencies and smaller for the high frequencies), and, third, a saturating nonlinearity in each component of the rotated and weighted domain.

Fig.1-left illustrates the 2-pixel image space in normalized luminance units in the  $[0,1]$  range. Each rectangle with two gray levels shows the corresponding 2-pixel image that lives at that point of the space. In this setting, the diagonal direction represented by the arrows in black is the *average luminance* direction. The direction represented by the arrows in blue is the *contrast* direction. Note that in this illustration of 2-pixel images, we sampled images at constant steps in both luminance and contrast directions. This helps to more easily see the nonlinear deformation of the response space shown in Fig.1-right. In Fig.1-right we show the 2-pixel example images being transformed by  $S$ . The linear transform  $W$  of  $S$ —a Fourier transform—is just a 45 degrees rotation: see the new orientation of

<sup>1</sup>A matlab implementation of this illustrative model can be downloaded from <http://isp.uv.es/code/visioncolor/noise.html>.

<sup>2</sup>A rotation for the linear transform makes sense because perceptually plausible domains include orthonormal transforms, i.e. rotations, as for instance local Fourier-like or local DCT-like receptive fields ([Watson, 1993](#)) or orthonormal wavelets ([Laparra et al., 2010](#); [Malo and Laparra, 2010](#)). In fact, the Fourier transform in a 2D vector space is just a 45 degree rotation, which is the rotation used in this toy example.

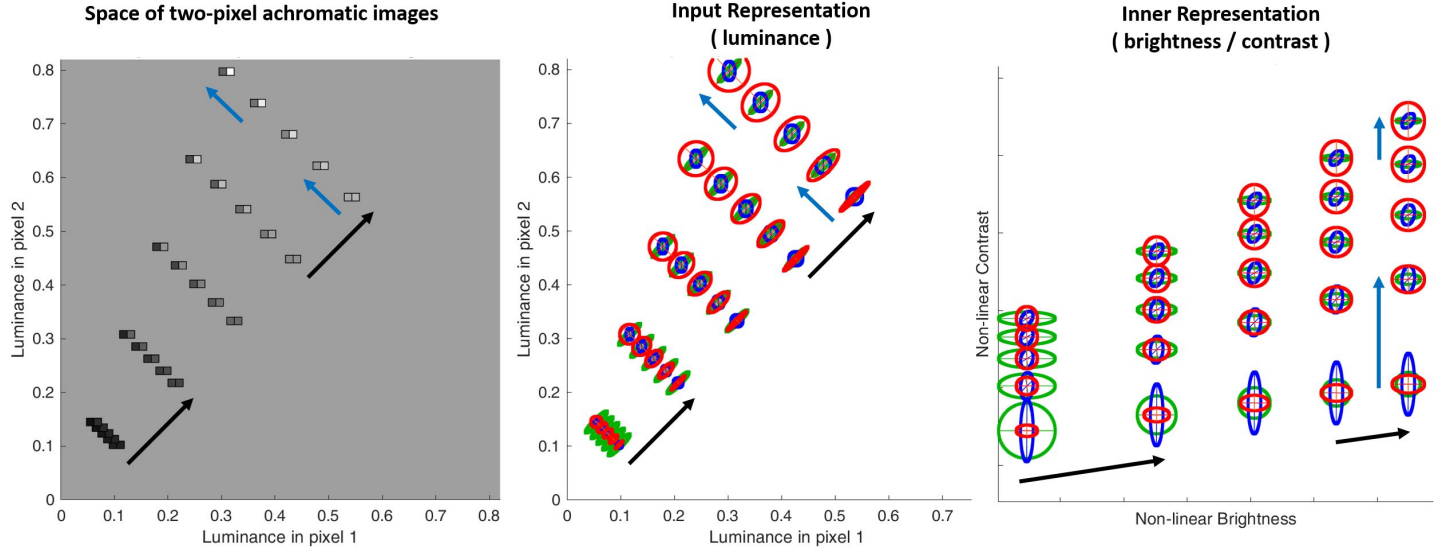


Figure 1: **Noisy vision model for 2-pixel images (the toy example)**. *Left*: Space of 2-pixel images with some examples uniformly separated in luminance (black arrows) and Michelson contrast (blue arrows). *Center*: Space of 2-pixel images with ellipsoids that represent the uncertainty introduced by the different factors considered in this work: *external noise* in green, *early noise* in blue, and *late noise* in red. *Right*: Response space corresponding to two sensors: *average brightness* in the horizontal axis, and *perceived contrast* in the vertical axis. The three noise sources are also represented in the response domain with the same colors. Please note that the relative sizes of the noises is changed by the nonlinearities of transform  $S$ . Thus depending on the stimulus properties, e.g. contrast versus luminance, different noise sources may have a larger effect on the discriminability in the response domain. See text for details.

the arrows in *black* and *blue*, and note that the new axes do represent the *average brightness* of the images (increasing to the right) and the *perceived contrast* (which increases upwards). The CSF weights that are applied after  $W$  attenuate the *high frequency* (or contrast) direction, are not visible in Fig.1-right because we hide the (arbitrary) units of the axes in the response domain. We do so because these arbitrary units are less informative than the non-uniform distances (arrow-lengths) that represent the deformation of the domain due to the masking nonlinearities. Note that in the response domain, or inner representation, once the saturating nonlinearities are applied in each axis, the euclidean distance between stimuli is not the same anymore. The distance between low-luminance stimuli is relatively increased while the high-luminance stimuli are transformed to be closer together (see lengths of arrows in black). This is consistent with Weber’s law (brightness vs luminance relation) (Fairchild, 2013). Similarly, the distance between the low-contrast stimuli has increased while the high-contrast stimuli are closer together in the vertical direction (see length of arrows in blue). This is consistent with the reduced discriminability of high-contrast stimuli (Legge and Foley, 1980; Legge, 1981). The transformation of distances—or metric matrices—resulting from  $S$  depends on the Jacobian of the deterministic transform  $S$ . For an abstract geometric explanation see Dubrovic et al. (1982), for examples in vision science see Malo (1999); Epifanio et al. (2003); Malo and Simoncelli (2006); Laparra et al. (2010). We will return to metric transformations in detail in Section 3.1 and Appendix A.

In the following we now address the noise sources and their associated uncertainties. Fig.1-center and Fig.1-right show ellipsoids corresponding to the different noise sources we consider here, either in the image space (center) or in the response space (right). Noise sources are represented as ellipsoids because none of the considered sources is *white*: they have different variance in different directions of the image or the response domains. White noise would be represented by spheres (circles in 2D) with radius proportional to the standard deviation. In case of *colored* (or *pink*) noise, we have ellipsoids determined by the corresponding covariance matrix—as we assume and model here.

In our illustration the ellipsoids in *green* represent the external noise (the one controlled by the experimenter). The ellipsoids in *blue* represent the early noise in the photoreceptors (or in the directions of the luminance axes, because each pixel is a photoreceptor). And finally, the ellipsoids in *red* represent the late noise: the noise in the brightness and contrast sensors, i.e. the noise in the axes of the response representation. In the following paragraphs we explore the different noise sources and their associated ellipsoids to understand them qualitatively.

First, the external noise (green ellipses) we chose is not white, but colored (or *pink*), i.e. with an  $1/f$  amplitude spectrum, inspired by [Henning et al. \(2002\)](#). The external noise thus has more energy (larger variance) in the low-frequency (average-luminance) direction and it has less energy (or variance) in the high-frequency (contrast) direction. Furthermore, it has the same covariance matrix (the same energy) for every stimulus or image across the stimulus space. Thus in the image space, the input representation, Fig.1-center, the green ellipses are elongated in the diagonal direction—more variance along low frequencies (luminance), black arrows, than high frequencies (contrast), blue arrows—and they have the same size everywhere<sup>3</sup>

Second, following [Brainard and Wandell \(2020\)](#), the early noise at the level of individual photoreceptors (blue ellipses) represent an independent Poisson-like noise: The width of the blue ellipsoids in the horizontal and vertical axes of the image space in Fig.1-center increases with luminance because the standard deviation of Poisson noise increases with the signal. Moreover, the alignment of the blue ellipses with the axes of the image space indicates that there is no correlation between adjacent photoreceptors—the Poisson-like noise is independent at every sensor.

The late noise, finally, is best initially inspected in the response domain, that is in Fig.1-right. We again chose a Poisson distribution for the late noise with no correlation over model units or “neurons”, following the conventional, simplest, assumption in neuroscience ([Dayan and Abbott, 2005](#)). The red ellipses are like the blue ellipses again in that they are aligned with the axes of the space, but here with the axes of the response domain, not the input domain: Their width increases (independently) with the responses of the model units, brightness and contrast. Of course, decorrelation over photoreceptors (for the early noise) and decorrelation over model units (for the late noise), is just something we selected for this toy illustration. More sophisticated correlations would correspond to changing the orientation of the corresponding ellipses, and hence having more parameters to fit when estimating the noise sources—not a fundamental difference, but added computational complexity.

The external and the early noises arise, and are defined, in the input (image) space while the late noise arises, and is defined, in the response domain. The shape of the external and early noises, their probability density functions, in the response domain (Fig.1-right) depends on the Jacobian of the deterministic transform  $S$ . An intuitive account of these transforms can be found in [Woods and Stark \(2011\)](#), and examples for the covariance matrices in vision science can be found in [Ahumada \(1987\)](#). This is the second piece of theory involved in our noise estimation methods which we detail in Section 3.1 and Appendix A. This allows us to compute the covariance matrices—and their associated ellipsoids—in different domains. Thus we can represent the ellipsoids—the magnitude of noise—of the three components of the noise (external, early and late) in both domains regardless of where they are actually arise or are defined.

Discrimination ability between stimuli will depend on two factors (the two pieces of theory mentioned above):

- **The distance in the response representation.** One may think of this as a weighted readout of the differences in each sensor response ([Graham, 1989](#)), or, more geometrically, as the use of a non-Eulidean metric in the response domain ([Malo, 1999](#); [Malo and Simoncelli, 2006](#); [Laparra et al., 2010](#)).
- **The uncertainty in the response representation.** Two stimuli  $\mathbf{x}_A$  and  $\mathbf{x}_B$  can be discriminated if their deterministic responses fulfill the following: Given one of the deterministic response vectors, say  $S(\mathbf{x}_A)$ , the other,  $S(\mathbf{x}_B)$  is far enough away from  $S(\mathbf{x}_A)$  such that it cannot be confused with the noisy version of the first, i.e.  $S(\mathbf{x}_B)$  cannot be confused with  $S(\mathbf{x}_A) + \mathbf{n}_{\mathcal{I}}(\mathbf{x}_A)$ . The marginal PDF of the noise in the direction of the departure determines the psychometric function and the discrimination

<sup>3</sup>In general, statistical properties of the external noise are something the experimenter may select to probe the system in certain ways. Note that changing the spatial spectrum of this external noise is equivalent to introducing correlations over the different locations and also changing the orientation of the green ellipses.

threshold (May and Solomon, 2013).

The analytical expression (and method) presented in Section 3 and the nonparametric method presented in Section 4 combine all the concepts illustrated in this toy example in a coherent form.

## 2.4 Experimental data used for modelling

We apply our proposed method to detection and discrimination data with well-controlled external noise reported by Henning et al. (2002). Henning et al. (2002) compared the detection and discrimination of standard sine gratings with so-called pulse-train stimuli, containing not only energy at the fundamental frequency—as in sine gratings—but equally much at all harmonics (within the limits of the display system). Both detection and discrimination experiments were repeated with and without added external pink ( $1/f$ ) noise.

We chose to model the data from Henning et al. (2002) because in their paper the authors argue that the pattern of results they obtained are consistent with the notion that low-contrast detection is limited by an early internal noise source but high-contrast discrimination is limited by late internal noise. They thus experimentally addressed the very same question we now believe to be able to address theoretically and computationally—hence we felt it was appropriate to use their data for our analysis.

## 3. Noise estimation I: Using only threshold data

### 3.1 Theory: perceptual distance in terms of thresholds and noise

The key of our proposal is to relate the psychophysical thresholds for detection and discrimination in presence (or absence) of external noise to a perceptual metric derived from a nonlinear model. In a discrimination experiment where a target stimulus  $\mathbf{x}$  is changed (“distorted”) in an arbitrary direction of the image space  $\Delta\mathbf{x}$ , experimental thresholds in that direction  $|\Delta\mathbf{x}|_\tau$  define an *empirical perceptual distance*, and following the qualitative reasoning of Section 2.3, we can use this empirical perceptual distance to determine a *theoretical perceptual distance* given an assumed model (transform  $S$ ). Maximization of the correlation between the experimental and the theoretical distances is the proposed method to obtain the relative magnitudes of the early and late noises, i.e. the parameters of the assumed noise sources for the considered deterministic model,  $S$ .

The (empirical) perceptual distance induced by a distortion in certain direction of the image space,  $\Delta\mathbf{x}$ , is proportional to the inverse of the discrimination threshold of departures in this direction  $\tau$ . That is:

$$D_{\text{emp}} = \frac{1}{|\Delta\mathbf{x}|_\tau} \quad (3)$$

A corollary of this formulation is that a large threshold—a large  $|\Delta\mathbf{x}|_\tau$ —is obtained when the perceptual distance in that direction is small, that is, in this direction the stimulus has to be changed or distorted a lot before an observer is able to discriminate the original from the changed or distorted stimulus.

However, the distance is not the only determinant of discriminability: In the current setting described by Eq. 1, discrimination between two stimuli,  $\mathbf{x}$  and  $\mathbf{x} + \Delta\mathbf{x}$ , will depend not only the difference between the corresponding deterministic responses ( $D_{\text{emp}}$ ), but also on the *inner noise*, the noise effectively limiting behaviour. Specifically, assuming a Euclidean read out, discrimination will be possible when the Euclidean distance in the inner representation,  $\Delta S = S(\mathbf{x} + \Delta\mathbf{x}) - S(\mathbf{x})$ , is larger than the standard deviation of the inner noise in the same direction.

Both Euclidean distance and noise thus determine discriminability. Both can be taken into account at the same time by using the Mahalanobis metric (Mahalanobis, 1936). The (non-Euclidean) theoretical perceptual distance,  $D_{\text{th}}$ , is thus given by the differences in the deterministic response,  $\Delta S$ , weighted by the covariance of the *inner noise*:

$$D_{\text{th}}^2 = \Delta S^\top \cdot (\Sigma_{\mathcal{I}})^{-1} \cdot \Delta S \quad (4)$$

where  $\Delta S = S(\mathbf{x} + \Delta\mathbf{x}) - S(\mathbf{x})$ , and  $\Sigma_{\mathcal{I}}$  is the covariance matrix of  $\mathbf{n}_{\mathcal{I}}$ .

In order to express this theoretical distance in terms of (1) the stimulus, and (2) the different noise sources—*external*, *early* and *late* noise—we invoke two known results as already introduced briefly above in section 2.3: First, the change of the perceptual metric matrix under deterministic transforms (Malo and Simoncelli, 2006), and, second, the change of the covariance of the noise under deterministic transforms (Ahumada, 1987). Both of these two results use the Taylor approximation of the nonlinear behavior of the system,  $S$ . This assumption is correct if the nonlinearity of the system is moderate, or if the noise is small-ish relative to the signal (low-noise limit).

Applying (Malo and Simoncelli, 2006) and (Ahumada, 1987) to equation 4, we see how the different noise sources contribute to the theoretical perceptual distance induced by a variation in the stimulus  $\Delta \mathbf{x}$  (see Appendix A):

$$D_{\text{th}}^2 = \Delta \mathbf{x}^\top \nabla S^\top \left( \underbrace{k^2 \Sigma_l}_{\text{late noise}} + \underbrace{k^2 \nabla S \Sigma_e \nabla S^\top}_{\text{early noise}} + \underbrace{2k^2 \mathbb{E}[\mathbf{n}_l \mathbf{n}_e^\top \nabla S^\top]}_{\text{corr. late-early}} + \overbrace{\underbrace{\nabla S \Sigma_e \nabla S^\top}_{\text{external noise}} + \underbrace{2k \nabla S \mathbb{E}[\mathbf{n}_e \mathbf{n}_e^\top \nabla S^\top]}_{\text{corr. early-external}} + \underbrace{2k \mathbb{E}[\mathbf{n}_l \mathbf{n}_e^\top \nabla S^\top]}_{\text{corr. late-external}}}_{\text{external dependent}} \right)^{-1} \nabla S \Delta \mathbf{x} \quad (5)$$

where  $\nabla S$  is the Jacobian of the model at  $\mathbf{x}$  and the matrix  $\Sigma_l$  is the covariance of the late noise  $\mathbf{n}_l$  at the point  $S(\mathbf{x})$ . The term that depends on  $\Sigma_e$  describes the early noise at  $\mathbf{x}$  propagated up to the response domain. In addition, we introduced an arbitrary scale factor,  $k$ , on all the *internal* noise sources (early and late) to indicate the critical role the *external* noise with covariance  $\Sigma_e$  plays to obtain the scale of the uncertainties—we will return to this issue below. The terms with the expected value,  $\mathbb{E}[\cdot]$ , in them, are all zero in case of independent noise sources. However, if noise sources are dependent the terms with  $\mathbb{E}[\cdot]$  are non-zero. In general they are not zero: for instance, in the conventional Poisson choice we have made here, the different noises depend on the signal and thus the cross correlation matrices do not vanish. The cross correlation terms imply that the covariance of the sum of the contributions to the internal noise is not simply the sum of individual covariance matrices. The proper *combination* of the noise sources has to be calculated.

### 3.2 Generality of Eq. 5 and derivation of classical expressions as special cases

Equation 5 is entirely general since it makes no assumption on the nature of the noise sources nor on its independence. Moreover, it can be applied to any model  $S$ —thus equation 5 holds for more complex (spatial vision) models than the one we consider here and introduced in section 2.2. It also holds if one were to explore different internal and external noises than the Poisson and pink noises we consider here (and in the particular cases further developed in Appendix A). The validity of equation 5 is only tied to the Taylor expansions in (Malo and Simoncelli, 2006; Ahumada, 1987), and these expansions are reasonable in case of low noise and moderately non-linear systems.

From our general expression in equation 5 one may deduce classic special cases if one considers the appropriate restrictions in the system and in the noise sources. One such special case is that of Burgess and Colborne (1988): A linear shift-invariant systems *without* early noise, and stationary and signal-independent *external* and *late* noises. In our terminology in Burgess and Colborne (1988) we have zero early noise,  $\mathbf{n}_e = 0$  and the late noise  $\mathbf{n}_l$  is not Poisson but is constant, e.g. Gaussian with constant variance independent of the input  $\mathbf{x}$  to the system  $S$ . This considerably simplifies equation 5 as all terms with  $\mathbf{n}_e$  vanish as well as all those with  $\mathbb{E}[\cdot]$ .

Moreover, we can derive the special case for a linear shift-invariant system in the Fourier domain. For such a system, its Jacobian can be written as  $\nabla S = F^\top \cdot \lambda \cdot F = \nabla S^\top$ , where  $F$  is a matrix with the Fourier basis functions (in rows), and  $\lambda$  is a diagonal matrix with the weights that are applied to each spatial frequency (the filter that represents the system). The covariance of stationary noises which do not depend on the signal can be formulated in the Fourier domain as well:  $\Sigma_e = F^\top \cdot N_e \cdot F$  and  $\Sigma_l = F^\top \cdot k^2 N_l \cdot F$ , where  $N_e$  is a diagonal matrix with the energy spectrum of the external noise, and  $k^2 N_l$  is the corresponding energy spectrum of the late noise (where we kept the scaling factor  $k$  to denote its amplitude).

Introducing the above special cases in Eq. 5, taking  $\Sigma_e = 0$  and  $\mathbf{n}_e = 0$ , using the orthogonality of the Fourier matrix, and considering the values (in the Fourier domain) in the diagonals of  $\lambda$ ,  $N_l$  and  $N_e$ , we finally have:

$$D_{\text{th}}^2 = \Delta \mathbf{x}^\top \cdot F^\top \cdot \left( \frac{\lambda^2}{k^2 N_l + \lambda^2 \cdot N_e} \right) \cdot F \cdot \Delta \mathbf{x} \quad (6)$$



which is equivalent to equation (1a) in [Burgess and Colborne \(1988\)](#).

### 3.3 The special role of the external noise

Another interesting feature of Eq. 5 is that it highlights the critical role of the external noise as a control parameter (or *reference*) to determine the scale of the other noise sources in the system (the ones object of our study). In absence of such control reference, the other noise sources could be arbitrarily scaled with no impact on the correlation between theory and experiment.

Note that if no external noise is used in the experiments, the term that does not depend on  $k$  vanishes. As a result, the perceptual distance reduces to:

$$D_{\text{th}}^2 = k^{-2} \left( \Delta \mathbf{x}^\top \nabla S^\top (\Sigma_t + \nabla S \Sigma_e \nabla S^\top + 2\mathbb{E}[\mathbf{n}_t \mathbf{n}_e^\top \nabla S^\top])^{-1} \nabla S \Delta \mathbf{x} \right)$$

and this means that an arbitrary scaling  $k$  of the size of the noise sources only leads to a corresponding scaling  $k^{-2}$  of the theoretical distance, which has no effect in the correlation between  $D_{\text{th}}$  and  $D_{\text{exp}}$ .

As a consequence, by maximizing the correlation with no external noise one could fit the structure of the covariance of the noise sources, but not its absolute scale, which would be of limited interest.

The sum of terms in Eq. 5 implies that the different noise sources actually play the role of relative references for each other: global scaling of all the noise sources at the same time has no effect on the correlation, but considering a bigger contribution (say of late noise) with no variation of the other sources, would have an impact in reproducing the experiments.

This observation suggests that the experiments used to determine the noise should use substantial amount of external noise and include early noise in the formulation to ensure the necessary constraints for the scale of the late noise and even noise at the decision stage. This is the reason to use accurate threshold measurements in external noise such as those in ([Henning et al., 2002](#)).

### 3.3 Practical estimation and results

Our proposal for noise estimation stated in section 2.2 consists of finding the noise parameters that maximize the correlation between  $D_{\text{exp}}$  (Eq. 3) and  $D_{\text{th}}$  (Eq. 5, which depends on the noise). In principle, given  $n$  experimental conditions to measure  $n$  thresholds, this optimization reduces to computing  $\frac{\delta D_{\text{th}}^i}{\delta \theta}$ , where  $\theta$  are the noise parameters and  $D_{\text{th}}^i$  is the distance for the  $i$ -th experimental condition, with  $i = 1, \dots, n$  ([Martinez et al., 2018](#)).

However, the inverse in Eq. 5 poses serious computational problems. Note that the derivative of the distance depends on the derivative of the metric, and the inverse implies a dependence on  $(\Sigma_{\mathcal{I}})^{-2}$ . Computing these inverses of huge matrices in every iteration of the optimization is unfeasible in practice<sup>4</sup> unless strong restrictions in the nature of the noise are assumed<sup>5</sup>.

Therefore, while the parametric expression presented above, Eq. 5, is convenient to understand the problem (for instance to link it to the classical results, or to understand the relevance of the external noise as a scaling factor for the unknowns), in practice, the optimization is easier by taking a nonparametric computation of the theoretical distance. As a result, in order to compute the perceptual distance between  $\mathbf{x}$  and  $\mathbf{x} + \Delta \mathbf{x}$  from noise, instead of Eq. 5, we propose to take the average Euclidean distance between the noisy responses,  $\mathbf{y}(\mathbf{x})$  and  $\mathbf{y}(\mathbf{x} + \Delta \mathbf{x}) = \mathbf{y}(\mathbf{x}) + \Delta \mathbf{y}$ :

$$\begin{aligned} D_{\text{th}}^2 &= E \left[ \Delta \mathbf{y}^\top \cdot \Delta \mathbf{y} \right] \\ &= E \left[ |\Delta S + \mathbf{n}'_{\mathcal{I}} - \mathbf{n}_{\mathcal{I}}|^2 \right] \end{aligned} \quad (7)$$

<sup>4</sup>Note that dealing with  $64 \times 64$  images and a 3-scales and 4-orientations steerable transform implies working with metric matrices of size  $25664 \times 25664$ . Optimization takes about 20-50 iterations and in each iteration we need to compute  $n$  of such inverses (one per data point).

<sup>5</sup>For instance, if late noise is assumed to be independent of early noise -true in the low-noise limit-, and we have restricted Poisson (i.e. only depending on the global energy of the response and not on the energy of each coefficient), the covariance of the transformed input noise can be diagonalized, the corresponding orthogonal matrices can be extracted from the inverse and the inverse reduces to inverting a diagonal matrix. *This is what we did for the results presented in June 2019 -Eqs. 8 and 9 in `job-latex-draft3.tex`-, but of course is a too restricted case*

where  $\Delta S = S(\mathbf{x} + \Delta\mathbf{x}) - S(\mathbf{x})$  is the difference between the deterministic responses, and  $\mathbf{n}_{\mathcal{I}}$  and  $\mathbf{n}'_{\mathcal{I}}$  are different realizations of the inner noise at the points  $S(\mathbf{x})$  and  $S(\mathbf{x} + \Delta\mathbf{x})$ , respectively. Note that Eq. 7 means that, when judging the difference between two stimuli, the brain compares two noisy responses:  $S(\mathbf{x}) + \mathbf{n}_{\mathcal{I}}$  and  $S(\mathbf{x} + \Delta\mathbf{x}) + \mathbf{n}'_{\mathcal{I}}$ .

In Appendix B we show the derivatives of the correlation between experimental and theoretical distances with regard to the noise parameters from Eq. 7. In this non-parametric case, the derivatives wrt noise do not involve matrix inversion, and hence they are easy to compute. This allows a practical optimization of the noise parameters (no matter the complexity of the noise) whenever  $\nabla S$  is easy to compute.

Eq. 7 also implies the relevance of input (external and early noise) as a scale factor for the late noise. However, this relevance is not that obvious in this expression because it is hidden in the distribution of the samples of the inner noise  $\mathbf{n}_{\mathcal{I}}$ . The relevance can be seen analytically in this particular case: if the inner noise distributions are symmetric -zero skewness- (which is reasonable under mild nonlinearities) and we impose zero distance for  $\Delta\mathbf{x} = 0$  (which is an obvious linear recalibration of the distance), in Appendix D we show that Eq. 7 reduces to  $D_{\text{th}}^2 = |\Delta S|^2 + |\mathbf{n}'_{\mathcal{I}}|^2 - |\mathbf{n}_{\mathcal{I}}|^2$ . In that case, as the realizations of the inner noise depend on the late noise and on the input noise, we have:  $\mathbf{n}_{\mathcal{I}} = \mathbf{n}_l(S(\mathbf{x})) + \nabla S \cdot \mathbf{n}^{\text{ee}} + \mathbf{n}_l(\nabla S \cdot \mathbf{n}^{\text{ee}})$ . Therefore, for a fixed difference in response,  $\Delta S$ , the interesting (anisotropic) behavior of the distance in different directions comes from the anisotropy of the noise. If there is no input noise (i.e.  $\mathbf{n}^{\text{ee}} = 0$ ) then one could scale the late noise by an arbitrary factor  $k$  and get the same anisotropy. Therefore, this scaling factor would have no effect in the correlation, and hence the global scale of the late noise would be arbitrary. This is easily avoided by using some external non-spherical noise, for instance pink noise as in (Henning et al., 2002), in the experiments.

On top of the observation of the relevance of external and early noise also in Eq. 7, Appendix C shows the equivalence in the anisotropy found through the parametric distance, Eq. 5, and the non parametric distance Eq. 7, which has more convenient derivatives. As a consequence, for computational convenience, we chose this specific non-parametric definition to get the parameters of the noise.

Using the data and model considered in Section 3 and the computationally convenient noise-dependent distance described in Eq. 7, we looked for the noise parameters that maximize the correlation between theory and experiment. In our case we assumed Gaussian-Poisson noise applied independently to every photodetector (early noise) and to every sensor at the saturated wavelet representation (late noise). The corresponding covariances of the noise are given in Appendix A. These covariances were used to generate noisy inputs and responses in the non-parametric computation of the distances.

Fig. 2 shows the correlations obtained when the noises are assumed to be purely Poisson (with no Gaussian component, and hence  $\alpha_e = \alpha_l = 0$ ). The blue-to-yellow color scale represents low-to-high correlations between theory and experiment. We used all the experimental detection and discrimination data using pulse-trains and sinusoids of different frequencies in external pink noise and with no external noise. We fitted the results of both observers at the same time. The figure shows the best (maximum correlation) scatter plot.

Fig. 2 illustrates the basic problem found in the determination of the noise parameters from the thresholds: the uncertainty of the optimum is large because the correlation surface is very flat. This problem is also found even if a different set of noise parameters is considered for each individual observer (see separated results per observer in Appendix D). When compared to the results in the next section, the use of restricted information (just thresholds as opposed to all the information in the psychometric functions) implies looser constraints and hence bigger uncertainties in the result.

### 3.3 Interim conclusions

The proposed expression for the theoretical distance, Eq. 5, has two interesting consequences:

- It generalizes the classical result in (Burgess and Colborne, 1988).
- It points out the special role of the noise at the input. Some noise at the input (either *external noise* or *early noise*) is necessary to find the scale of the *late noise*.

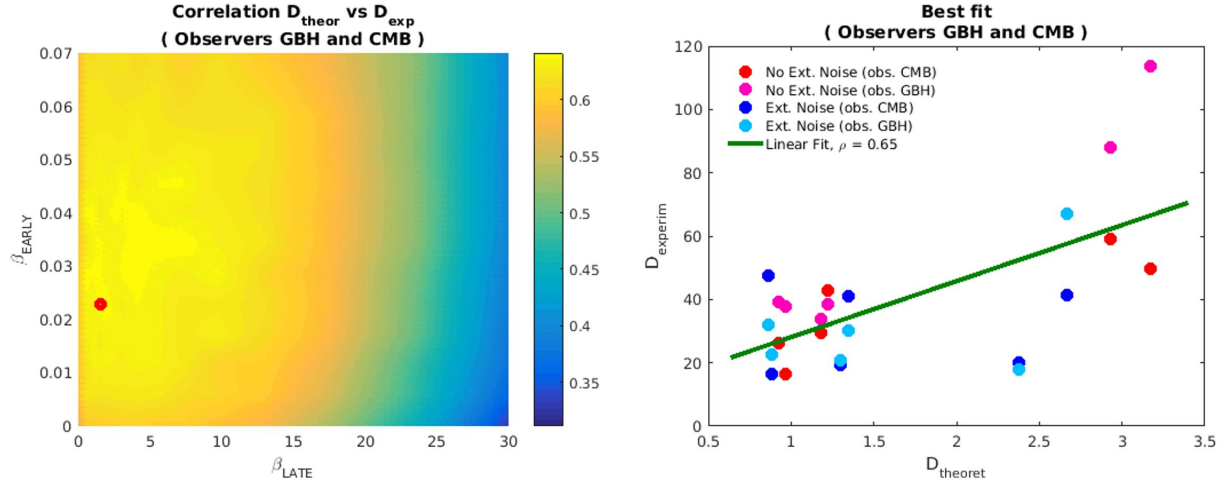


Figure 2: **Early and late noise parameters from threshold data.** The left plot displays the correlation between the theoretical distance (based on the noise) and the experimental distance (based on the thresholds). The optimal parameters, here highlighted in red, are those that maximize the correlation ( $\beta_e = 0.023$ ,  $\beta_l = 1.52$ ). The plot at the right shows the best (maximum correlation) scatter plot for the different observers and conditions: with no external noise, in red, and with external noise, in blue. In this optimal case the Pearson correlation is 0.65. The correlation drops to 0.64 and 0.61 if one neglects either early noise or late noise respectively.

## 4. Noise estimation II: Using full psychometric functions

In this section we follow the suggestion of Green and Wichmann (1999) ? on the importance of full psychometric functions and not only thresholds for modelling behavior. In particular, we here show that if the full psychometric function is used, there is no need to use external noise in order to scale the size of the early and late noises.

Specifically, we use the definition of the psychometric function in terms of the density of the internal noise given in (May and Solomon, 2013): the probability of correct detection of a variation  $\Delta x$  over the stimulus  $x$  is given by the cumulative density function of the internal noise in the direction of variation of the stimulus,

$$P_{\text{correct}} = \frac{1}{2} + \int_0^{|\Delta x|} p(\mathbf{u}^\top \cdot \mathbf{n}_{\mathcal{I}}^x) \mathbf{u}^\top \cdot d\mathbf{n}_{\mathcal{I}}^x \quad (8)$$

where  $p(\mathbf{u}^\top \cdot \mathbf{n}_{\mathcal{I}}^x)$  is the probability density function (PDF) of the noise in the internal representation expressed in the input domain and projected in the direction of variation of the signal,  $\mathbf{u} = \frac{\Delta x}{|\Delta x|}$ . Figure 3 illustrates this concept in the input domain (the two-pixel image space described in Fig. 1). In this context, the departures from a certain background or pedestal  $x$  in certain direction  $\Delta x$  will be visible when the size of the departure can be discriminated over the noise in that specific direction, and this is related to the cumulative density function (CDF) of the noise in that direction (i.e. Eq. 8).

### 4.1 Estimation

Given a response model that includes noise, e.g. Eq. 2, and certain experimental conditions (increments  $\Delta x$  over certain pedestals  $x$ , as the data by (Henning et al., 2002) considered in Section 2.4), the parameters of the noise can be estimated from the best reproduction of the psychometric functions. Specifically, the model is used to generate noisy responses for the considered stimuli and certain noise parameters. Then the model is used to express the noisy responses back in the input domain. The cumulative histograms of the noisy samples in the direction of the signal variation are the prediction of the experimental psychometric functions for the considered noise parameters. Note for instance that at certain point (or stimulus) in Fig. 3 a smaller/bigger amount of noise or a different orientation of the

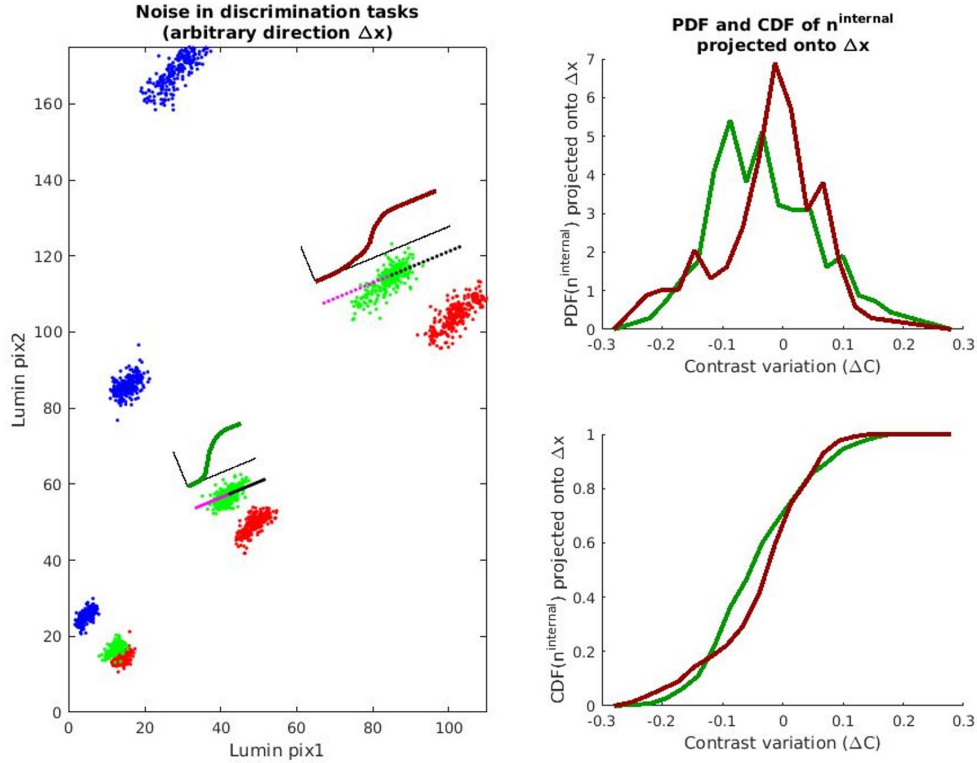


Figure 3: **Psychometric functions depending on the internal noise expressed in the domain  $x$**  (probability of correct detection of the variation  $\Delta x$  over  $x$ ). In the left plot we show the 2-pixel image space as described in Fig. 1. In this space we show samples of the noisy internal responses of nine stimuli of different luminance (along the diagonal direction) and different contrast (along the perpendicular-to-the-diagonal direction). For two scatter plots (in green), we represent departures from the average  $x$  in a specific direction  $\Delta x$ : along the lines in black and pink. The sigmoids in green and brown represent the CDFs of the noise projected onto the direction of variation of the signal. The plots at the right represent the PDFs (top-right), and CDFs (bottom-right) for the two considered clusters. Note how the CDF in brown squeezes when expressing the abscissa in contrast units (by dividing the variation by the average luminance).

multivariate PDF would lead to more sharp/smooth predictions for the corresponding psychometric function. In this case (as opposed to the case in Section 3 where we only used the threshold information) here there is no need of external noise to scale the results. Here the modification of the parameters of the internal noise directly lead to scaled predictions.

In that way, exploring a range of noise parameters and computing the errors in predicting the psychometric functions, we get the noise that better explains the experimental functions (with no need of measurements in external noise).

## 4.2 Results

The color surfaces in Figure 4 show the prediction errors for a range of early and late noise parameters obtained with the above procedure for the psychometric function data of the two observers in (Henning et al., 2002). We just used the experiments with no external noise. The blue-to-yellow color scale represents low-to-high prediction error. The optimal noise parameters (minimum error) are highlighted in red. The experimental data of the psychometric functions are given by the blue dots of the plots, and the curves represent different predictions from Eq. 8, the considered model and the purely Poisson noises. The curves in black correspond to the optimal predictions for each observer using both early and late noise. The curves in red and green (which clearly lead to worse predictions of the experimental data) come from disregarding early noise and late noise respectively.

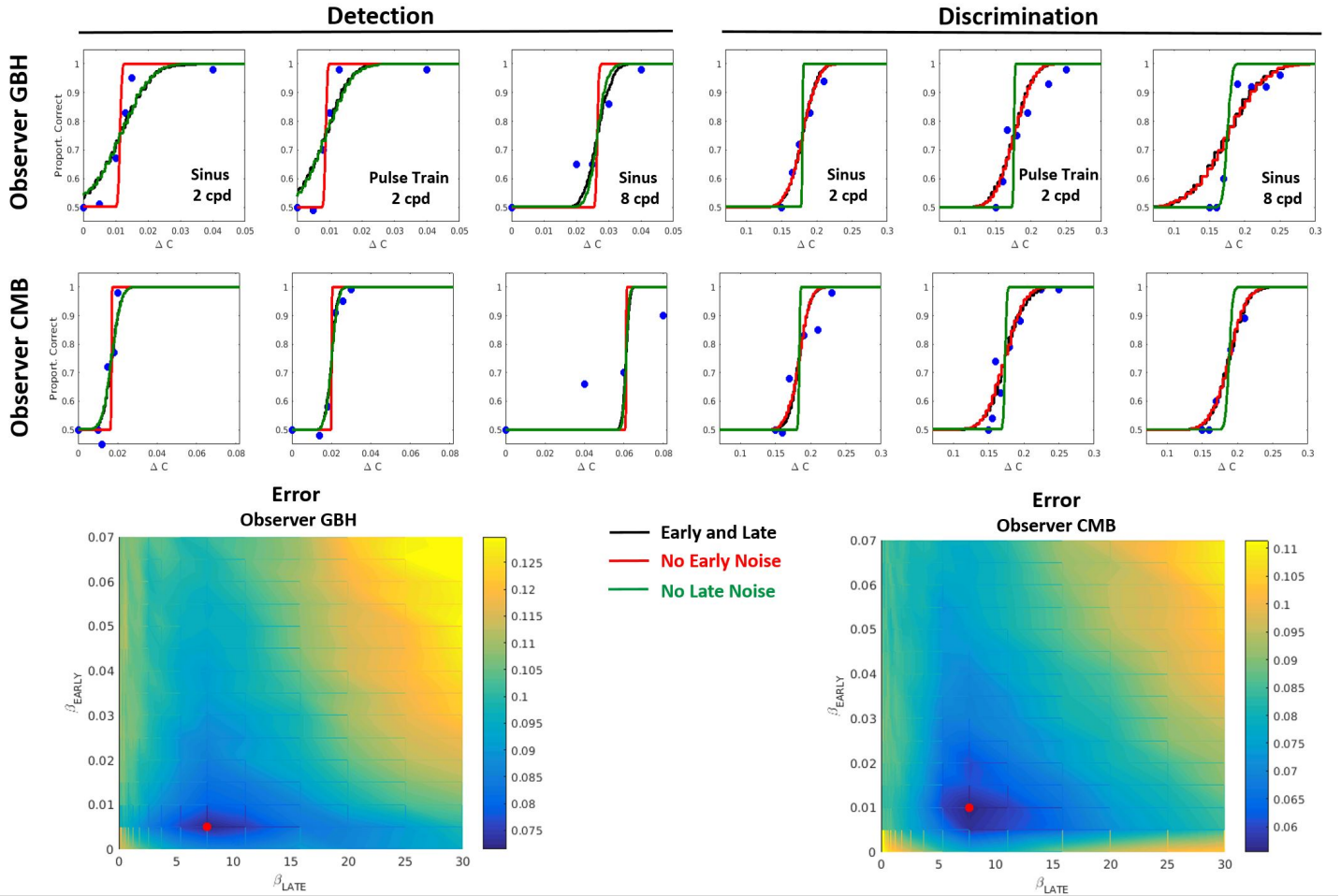


Figure 4: **Early and late noise parameters using full psychometric functions.** The color surfaces represent the average RMSE error in reproducing the psychometric function through the Cumulative Density Function of the noise in the direction of the test. In each case the optimum is given by the minimum in the error surface. For the observers GBH and CMB the optima, highlighted in red, are located in  $(\beta_e = 0.005, \beta_l = 7.69)$  and  $(\beta_e = 0.01, \beta_l = 7.69)$  respectively. The plots at the top represent the experimental data of the psychometric functions (blue dots) and different optimal predictions considering: both early and late Poisson noise (in black), only late noise (in red), and only early noise (in green).

These results imply consequences on the reliability of the methods for noise estimation and the role of the early and late noise sources.

**Reliability of the methods:** The accuracy of the estimation (given by the sharpness of the goal function at the optimum) is substantially higher for the full-psychometric method. Note the clear minima in Fig. 9 as opposed to the flat plateaus obtained in the threshold-only-method in Figs. 2 and 9. Moreover, the consistency between the results of the two observers is substantially higher in the full-psychometric method with regard to the threshold-only method (compare Fig. 4 and Fig. 9).

In summary, improved accuracy and consistency indicate that the full-psychometric method is more reliable than the threshold-only method.

**Role of the early and the late noise:** The consideration of both *early* and *late* noise sources is mandatory for a proper reproduction of the psychometric function over a range of visual conditions (both in detection and discrimination) given the different role of the noise

in these conditions.

Early noise seems particularly relevant in detection, where contrast is small and hence late noise is negligible given the small neural responses in the inner domain. In detection, neglecting the early noise leads to unrealistic (too sharp) psychometric functions (see curves in red). These predictions (according to the error surfaces) are not improved even if substantially bigger late noise is considered. On the contrary, early noise seems irrelevant to explain discrimination. In discrimination the neural responses are already high and hence the signal dependent contribution of late noise is much higher than the early noise transformed into the inner domain. Note that early noise is compressed by the saturating nonlinearity at high amplitudes in the inner representation,

Late noise seems particularly relevant in discrimination. If late noise is neglected in discrimination the predictions are unrealistic (too sharp), see curves in green. These predictions (according to the error surfaces) are not improved even if substantially bigger early noise is considered. On the contrary, late noise seems irrelevant in detection: note that the no-late-noise green curve matches the black curve in detection.

### 4.3 Understanding the role of early and late noise in detection and discrimination

In this section we generate noisy responses for gratings of 2 cycl/deg of different contrast (0.01, 0.15 and 0.7) and different average luminance (15, 50, 100)  $cd/m^2$  using the model in Eq. 2 and the results of the Poisson noise sources obtained with the full-psychometric method.

The corresponding distributions of the early and late noises both in the input domain and in the inner representation clarify the role of the contributions of these sources in detection and discrimination scenarios.

Figure 5 shows the noisy signals with different contributions of the noise in the input and the inner representations. Computations are done with a full scale model that works with  $256 \times 256$  images. However these two-dimensional projections are obtained by selecting 2 photoreceptors of the image representation and 2 sensors of the inner representation. For illustrative purposes, in the input we took photoreceptors corresponding to the darkest and lightest locations of the gratings, and in the inner representation we considered a wavelet sensor from the low-frequency residual and another tuned to the 2 cycles/deg band. In this way, the meaning of the representations in Fig. 5 is qualitatively similar to the representations in toy scenario presented in Fig. 1: the input spaces are totally equivalent, and in the projection that we consider here the horizontal axis also represents brightness responses and the vertical axis also represents the responses elicited by the contrast of the gratings.

In this context, the clusters of the samples corrupted by the early noise in the input domain (top-left plot) display the properties of the assumed Poisson noise in the photoreceptors: note that (1) the width (or variance) of the clusters increases with the luminance in each photoreceptor, and (2) the ellipsoidal clusters are aligned with the axes because we assumed no correlation between the noise in the different photoreceptors. Similarly, the late noise in the inner representation (middle-right and bottom-right plots) also displays the Poisson properties: the variance increases with the average and there is no correlation between the uncertainty in the different sensors. Interestingly, when the late noise is transformed back into the input representation (e.g. top-center plot) there is a strong correlation in the uncertainty of the different photoreceptors. The same is true in the case of the early noise in the inner representation (its covariance is non-diagonal) but it is not as easy to see in the clusters given the small scale of the early noise there (middle-left and bottom-left plots).

The interesting interaction between the Poisson nature of the noise sources and the nonlinearities of the model implies that in the inner representation (where decisions are made), different sources (early or late) determine the performance in different conditions (detection or discrimination). Note that the saturating nonlinearity in the contrast response implies that the clusters of early noise get compressed for progressively bigger contrasts (see that the red cluster is wider than the blue in the bottom-left plot). On the contrary, the Poisson nature of the late noise implies that the uncertainty due to this noise for the high contrast signals is bigger than the variability introduced for the responses to low contrast gratings (blue cluster is wider than the red in the bottom-right plot).

This is even more clearly represented in Figure 6: note that the PDFs of the early and late noise are basically the same for low

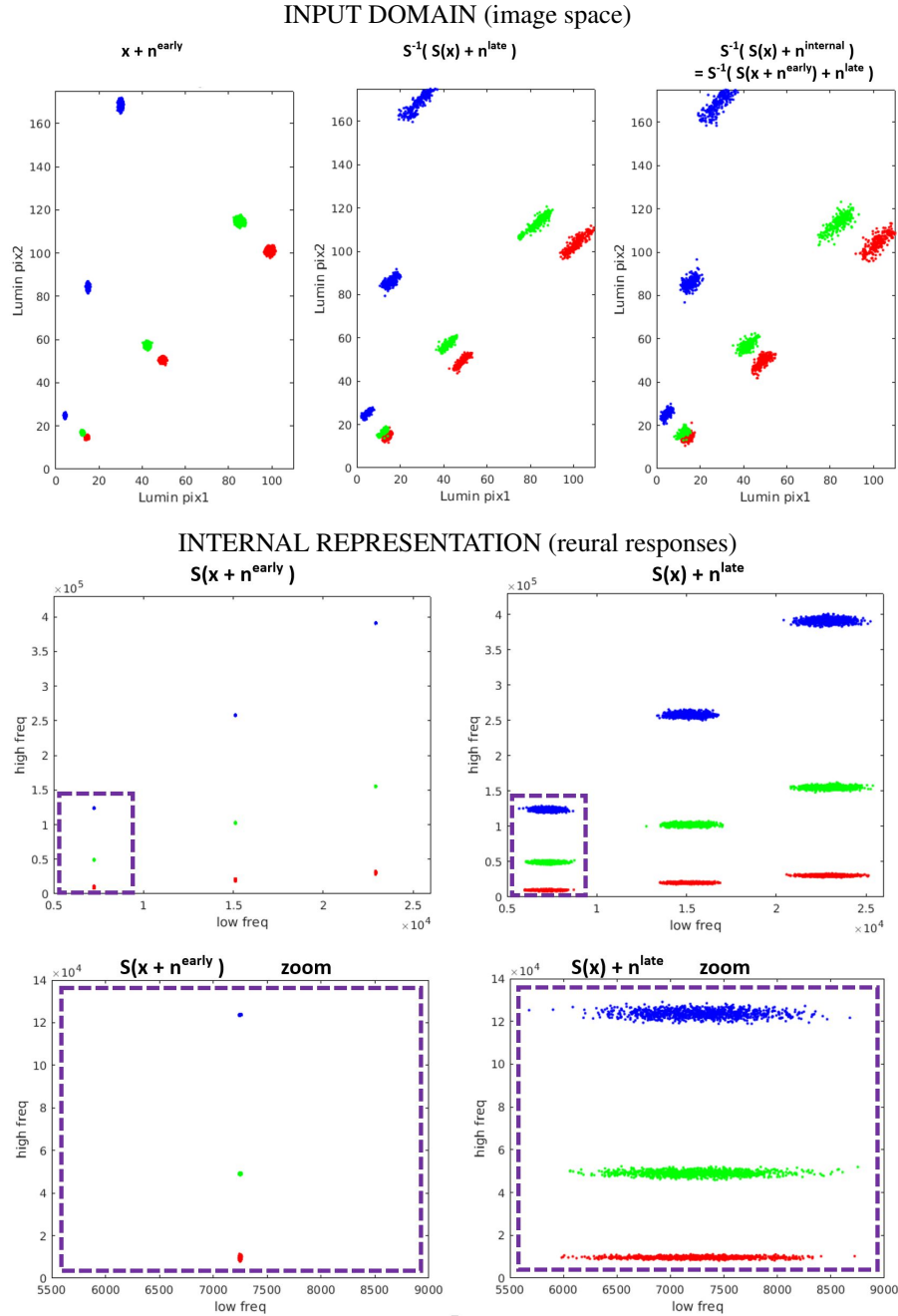


Figure 5: **Gratings corrupted by early and late noise with Fano factors estimated in section 4.2.** We show samples in 2-d perjections of the input domain (top row) and the internal representation (middle and bottom rows). The signal in the input representation corresponds to the brightest and the darkest locations of a 2cpd grating for different values of luminance and contrasts. Here, **red**, **green**, and **blue** clusters correspond to progressively higher values of contrast [0.01, 0.15, 0.7]. And clusters progressively further away from the origin in the diagonal direction of the input domain correspond to images with higher average luminance, with values [15, 50, 100]  $cd/m^2$ . The middle row shows the samples in the 2-dimensional representation given by a local sensor tuned to zero-frequency (horizontal axis) and by a wavelet sensor tuned to 2 cycl/deg (vertical axis). The rectangles in dashed style highlight the region of low-luminance gratings of different contrast. The bottom row zooms-in this region.

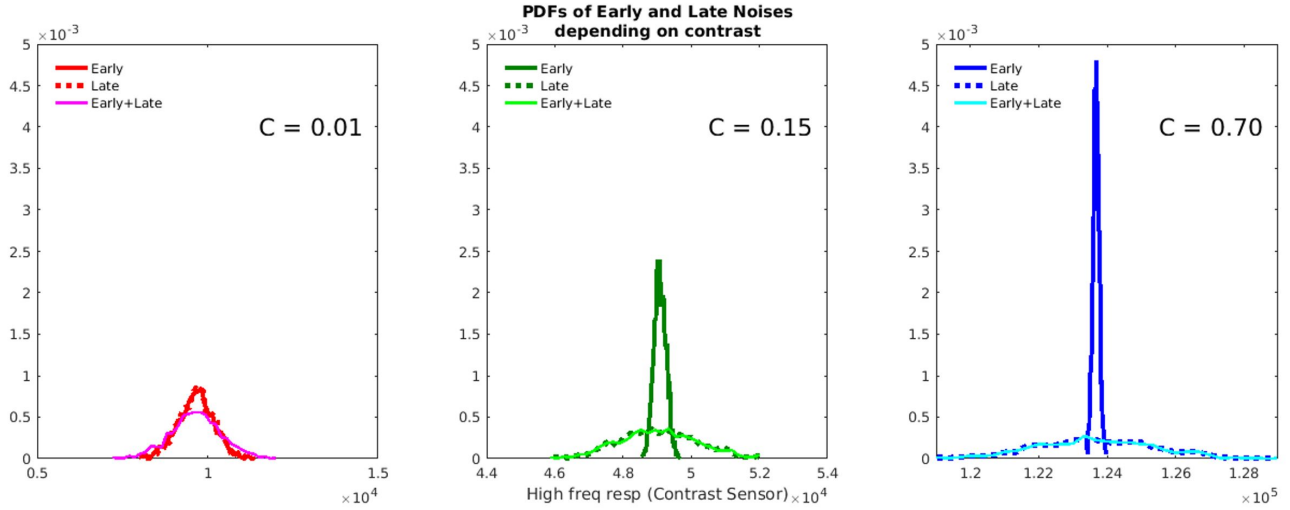


Figure 6: **Marginal PDFs of the early, late, and internal (early+late) noise sources in the inner representation.** These PDFs are computed from the samples of the 2 cycle/deg sinusoidal gratings of different contrast (with average luminance of  $15 \text{ cd/m}^2$ ) shown in the bottom row of Fig. 5. The marginals are taken in the direction of the sensor tuned to 2 cycl/deg (vertical axis in Fig. 5).

contrast ( $C = 0.01$ ), but when the contrast is increased the PDFs of the early noise are squeezed (solid curves) while the PDFs of the late noise widen (dashed curves). For low contrast gratings the noise is basically determined by the early component (and this effect would be even bigger for close-to-zero contrast used in actual detection experiments), while the width for high contrast is totally determined by the late noise.

This explains why the consideration of one noise source or the other is important to reproduce the experimental psychometric functions in Figure 4, and the different role of early and late noise in detection and discrimination.

## 5. Psychophysical versus physiological estimates of early noise

Our psychophysical estimates of the noise should have physiological correlates. One might think (naively) that our psychophysical estimate is directly related to the noise in the electrical response of L,M,S retinal cones. Similarly, one may think that our late noise could be related to the noise at the cortex. Nevertheless, here we show that direct comparison is not that simple.

Appendix E describes how we used ISETBIO (Brainard and Wandell, 2020) to get a reasonable physiological estimation of retinal noise. The discussion here will clarify why the comparison is not straightforward and why it is sensible to have one order of magnitude less noise in a psychophysical model.

Fig. 7 (top panel) shows the standard deviation of our estimated early and late noise sources on top of a sinusoid for different average luminance and different contrasts. The equivalent ISETBIO noise in  $\text{cd/m}^2$  is plotted on top for useful reference. Fig. 7 (bottom panel) shows sample images with ISETBIO noise and with the inner noise estimated by us, both back in the spatial domain.

If noise controls the discriminability, it should be just noticeable (or almost invisible) for the average observer. Clearly, that is not the case for the physiological noise in the retina: ISETBIO noise is too big and clearly visible. This indicates the presence of downstream mechanisms to remove this uncertainty (motion compensation + evidence accumulation over time + spatial low-pass filtering...). Interestingly our noise estimate is almost invisible on top of the background pattern. In order to explore its nature and assess its early/late components we show scaled versions of the noises on top of a flat background of  $60 \text{ cd/m}^2$ . While the Poisson early noise (trivially) inherits the spatial structure of the luminance, the late noise reveals a contrast/frequency dependence due to the inner working of the



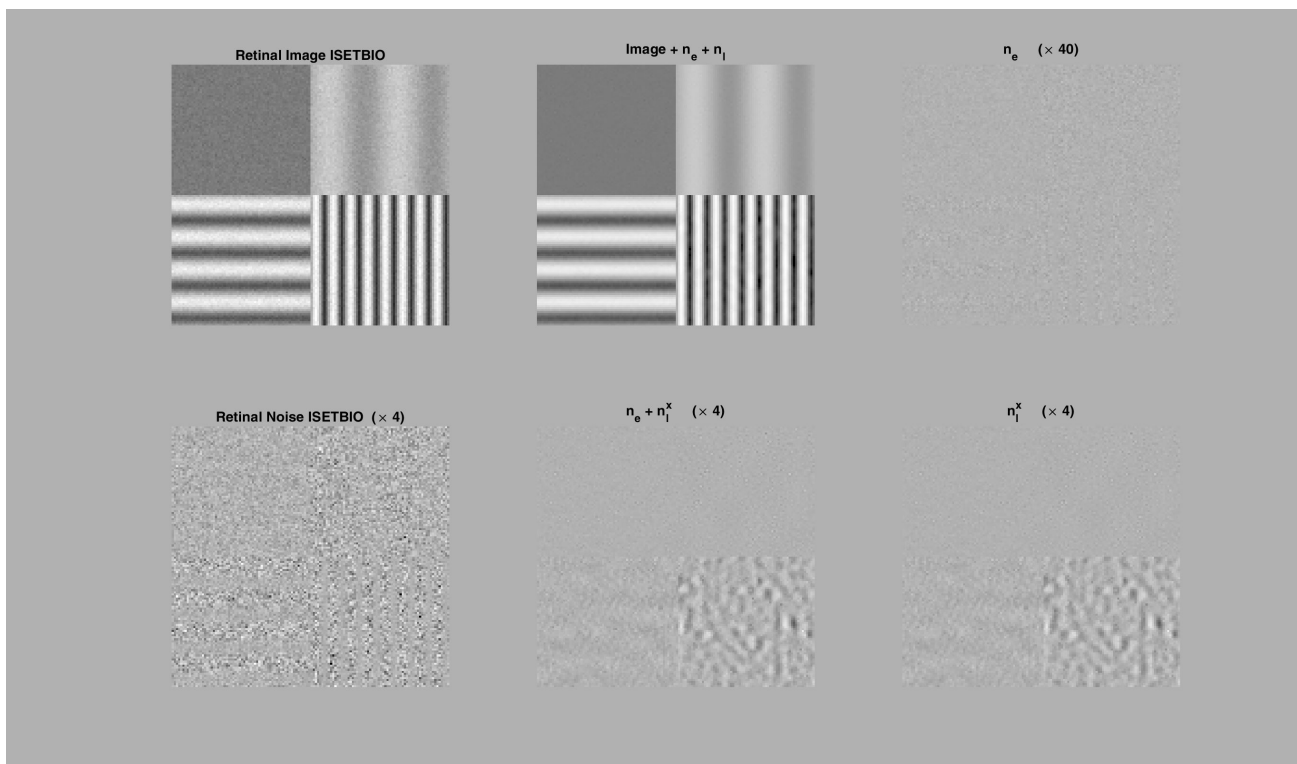
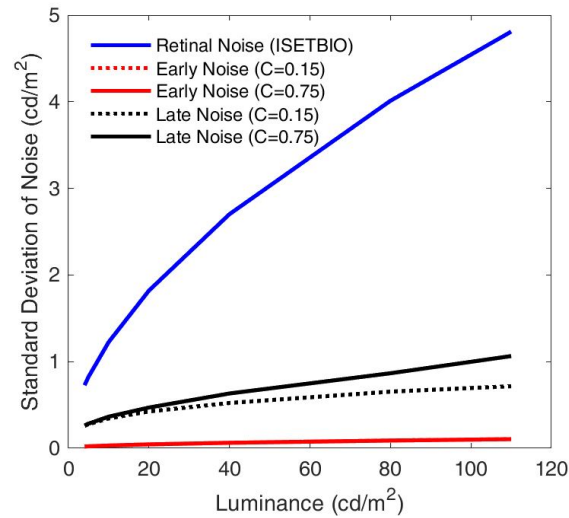


Figure 7: **Comparison of the physiological (retinal) noise estimated in Appendix E following (Brainard & Wandell, 2020), and the psychophysical (Early and Late) estimations proposed here.** *Top panel:* shows the standard deviation of the early and the late noises as a function of the luminance and contrast of a 4 cpd sinusoidal stimulus. As expected from the Weber-law, the noise increases with luminance. Moreover, according with masking, the late noise increases with contrast, which is not the case for early noise. The deviation of the physiological noise in the retina (see Appendix E) is plotted in the same units as a reference. *Bottom panel:* shows a representative stimulus calibrated in luminance with the inner noise of both models inverted back into the image space. Luminance of the flat square is  $30 \text{ cd/m}^2$ . Average luminance of the sinusoids is  $60 \text{ cd/m}^2$ . Frequencies are 2, 4 and 8 cpd, and contrasts are 0.25, 0.75, and 0.9 respectively.

nonlinear wavelet filters of the deterministic model. Note that more noise is allocated in the high contrast regions. This is consistent with the results in Fig. 5-(bottom right) and Fig. 6-right, that highlight the increase of the variance of late noise with contrast. Moreover, note also in Fig. 7 that the frequency of the noise depends on the frequency of the background pattern because more active sensors are more affected by the late noise. A final factor that affects the magnitude of the late noise in the input domain is the inverse of the CSF that enhances the amplitude of the (less visible) high-frequency noise.

## 6. Discussion

### 6.1 Noise in psychophysical models of early vision

**Draft (too preliminary) subsection:** talk about relative magnitude of early and late; discussion whether constant or not; explain how yoked to complexity of the model (cite auditory community who typically take different route than vision community).

Important: We assume Poisson noise early and late ... thus our paper does not talk to the debate about level-dependent late noise because we assume it! Larger exploration of different noises (Gaussian with fixed variance) early, late or both or combinations of fixed + varying as in (Wichmann, 1999) would need to be explored to address the question, but this is out of the scope here.

However, using our methods we believe one should be able to investigate the role of level-independent late noise in models of spatial vision (see e.g. Wichmann, 1999; Kontsevich et al., 2002; Georgeson and Meese, 2006b; Schütt and Wichmann, 2017), an issue we return to in the discussion.

### 6.2 Readout metric and noise at the decision stage

When there is noise at the decision stage or when the read out is not Euclidean, the proposed Eq. 5 changes as outlined below, but the relevance of the noise at the input to determine the scale of the different components of the noise mentioned above is still the same.

On the one hand, noise at the decision stage could be introduced at the distance:  $D_{\text{th}}^n = D_{\text{th}} + n_{\text{decision}}$ . But this is equivalent to an extra expansion of the uncertainty in the direction of stimulus modification, whatever this direction is, i.e. an extra isotropic noise. This isotropic noise is equivalent to including an extra diagonal term in the covariance of the inner noise:  $\Sigma_{\mathcal{I}} + k^2 \sigma^2 I$ . Again, the scale factor  $k$  of this isotropic noise could not be obtained with no external nor early noise.

On the other hand, a non-Euclidean readout of the variations of the response according to some *readout metric matrix*  $R$ , implies that  $D^2 = \Delta \mathbf{y}^\top \cdot R \cdot \Delta \mathbf{y}$ . With  $R$  symmetric it can be diagonalized by orthonormal transforms:  $R = B \cdot \lambda \cdot B^\top$ . Therefore, this a non-Euclidean metric in the response domain is equivalent to including an extra transform to a domain  $\mathbf{y}' = \lambda^{\frac{1}{2}} \cdot B^\top \cdot \mathbf{y}$  where the readout is Euclidean. The role of this extra transform (for the metric matrix) is similar in spirit to a whitening transform (for the covariance matrix). In this new domain, the covariance of the inner noise would be  $\Sigma_{\mathcal{I}_{\mathbf{y}'}} = \lambda^{\frac{1}{2}} \cdot B \cdot \Sigma_{\mathcal{I}} \cdot B^\top \cdot \lambda^{\frac{1}{2}}$ . Therefore, Eq. 4 can be generalized to:

$$D_{\text{th}}^2 = \Delta S^\top \cdot \left( \lambda^{\frac{1}{2}} \cdot B \cdot \Sigma_{\mathcal{I}} \cdot B^\top \cdot \lambda^{\frac{1}{2}} + k^2 \sigma^2 I \right)^{-1} \cdot \Delta S \quad (9)$$

where  $\Sigma_{\mathcal{I}}$  has the same expression as the one in Eq. 5, and, as a result, all the discussion around our first result, and specifically, the role of the external noise is the same: even if both factors (non-Euclidean readout and noise in the decision) are taken together, the scale of the late noise and the decision noise would remain unknown if there is no external noise at the input.

### 6.3 Experimental consequences: Maximum differentiation from noise estimates

The concept of Maximum Differentiation has been proposed as a way to decide between vision models (Wang and Simoncelli, 2008), or as a way to measure the free parameters of vision models (Malo and Simoncelli, 2015) using the associated perceptual distance. Originally (Wang and Simoncelli, 2008) proposed a method to generate stimuli maximally/minimally discernible by observers according to an iterative procedure of perceptual distance maximization/minimization. This, depending of the model may be extremely expensive. However, following the second order approximation of the non-Euclidean distance (as used in Appendix A (Malo, 1999;

(Malo and Simoncelli, 2006; Laparra et al., 2010)) the Maximum Differentiation method was simplified and reduced to the estimation of the eigenvectors of the discrimination ellipsoid (Malo and Simoncelli, 2015; Martinez et al., 2018).

The theory proposed here allows the estimation of the covariance matrix of the inner noise and hence the design of interesting stimuli in cardinal directions of the noise-dependent metric. Note that according to the transform of the covariance of noise along nonlinear networks (Ahumada, 1987), the directions of maximum and minimum discrimination in the spatial domain depend on the Jacobian of the model and the covariance of the noise in the input domain:

$$(\Sigma_T^x)^{-1} = \nabla S^\top \cdot \Sigma_T^{-1} \cdot \nabla S \quad (10)$$

Eigenfunctions of this covariance (where  $\nabla S$  and  $\Sigma_T^{-1}$  are point-dependent) lead to stimuli that can be used to check the effect of the noise components at different points of the image space (e.g. detection and discrimination).

## 6.4 Final remarks

The estimated variance of the early and late noise can be used for a more accurate account of the mutual information between the retinal image and the inner representation. With the proposed method realistic values for the noise could be obtained for any model, and hence the results in (Malo, 2020) on the information transmitted by spatial vs chromatic mechanisms or by linear vs nonlinear transforms could be more than rough estimates with reasonable noise assumptions. Similarly, better noise estimates could lead to an improvement of image quality measures such as (Sheikh and Bovik, 2006) based on modeling information transference along the visual pathway.

The proposed late-noise estimation procedure from experiments using early-noise may be used to modify the (inner noise or inner metric) assumptions in recent models of spatial vision (Schütt and Wichmann, 2017; Martinez et al., 2018), as well as to solve debates on the relative relevance of the noise and the nonlinearities of the models (Georgeson and Meese, 2006b).

## References

- Ahumada, A. J. (1987). Putting the visual system noise back in the picture. *J. Opt. Soc. Am. A*, 4(12):2372–2378.
- Brainard, D. and Wandell, B. (2020). *ISETBIO: tools for modeling the human visual system front end*. Imageval Consulting.
- Burgess, A. and Colborne, B. (1988). Visual signal detection, IV: Observer inconsistency. *JOSA A*, 5(4):617–627.
- Dayan, P. and Abbott, L. F. (2005). *Theoretical Neuroscience: Computational and Mathematical Modeling of Neural Systems*. The MIT Press.
- Dubrovin, B., Novikov, S., and Fomenko, A. (1982). *Modern Geometry: Methods and Applications*. Springer Verlag, New York.
- Epifanio, I., Gutierrez, J., and Malo, J. (2003). Linear transform for simultaneous diagonalization of covariance and perceptual metric matrix in image coding. *Patt. Recog.*, 36(8):1799–1811.
- Fairchild, M. (2013). *Color Appearance Models*. The Wiley-IS&T Series in Imaging Science and Technology. Wiley.
- Georgeson, M. and Meese, T. (2006a). Fixed or variable noise in contrast discrim.? the jury’s still out. *Vis.Res.*, 46(25):4294–4303.
- Georgeson, M. A. and Meese, T. S. (2006b). Fixed or variable noise in contrast discrimination? The jury’s still out. . . . *Vision Research*, 46(25):4294–4303.
- Graham, N. (1989). *Visual pattern analyzers*. Oxford University Press.
- Green, D. M. and Swets, J. A. (1988). *Signal Detection Theory and Psychophysics*. Peninsula Publishing.

- Henning, G., Bird, C., and Wichmann, F. (2002). Contrast discrimination of pulse trains in pink noise. *JOSA A*, 19(7):1259–1266.
- Kontsevich, L. L., Chen, C.-C., and Tyler, C. W. (2002). Separating the effects of response nonlinearity and internal noise psychophysically. *Vision Research*, 42(14):1771–1784.
- Laparra, V., Muñoz, J., and Malo, J. (2010). Divisive normalization image quality metric revisited. *JOSA A*, 27(4):852–864.
- Legge, G. (1981). A power law for contrast discrimination. *Vision Research*, 18:68–91.
- Legge, G. and Foley, J. (1980). Contrast masking in human vision. *Journal of the Optical Society of America*, 70:1458–1471.
- Mahalanobis, P. (1936). On the generalized distance in statistics. *Proc. Nat. Inst. Sci. India*, 2(1):49–55.
- Malo, J. (1999). *Redundancy reduction in the human visual system: new formulation and applications to image and video coding*. PhD Thesis, School of Physics, Univ. Valencia.
- Malo, J. (2020). Spatio-chromatic information available from different neural layers via gaussianization. *J. Math. Neurosci.*, 10(18).
- Malo, J. and Laparra, V. (2010). Psychophysically Tuned Divisive Normalization Approximately Factorizes the PDF of Natural Images. *Neural Computation*, 22(12):3179–3206.
- Malo, J., Pons, A., Felipe, A., and Artigas, J. (1997). Characterization of the human visual system threshold performance by a weighting function in the gabor domain. *Journal of Modern Optics*, 44(1):127–148.
- Malo, J. and Simoncelli, E. (2006). Nonlinear image representation for efficient perceptual coding. *IEEE Trans.Im.Proc.*, 15(1):68–80.
- Malo, J. and Simoncelli, E. (2015). Geometrical and statistical properties of vision models obtained via maximum differentiation. In *Proc. SPIE Electronic Imaging*, pages 93940L–93940L. International Society for Optics and Photonics.
- Martinez, M., Bertalmío, M., and Malo, J. (2019). In praise of artifice reloaded: Caution with natural image databases in modeling vision. *Front. Neurosci.* doi: 10.3389/fnins.2019.00008.
- Martinez, M., Cyriac, P., Batard, T., Bertalmío, M., and Malo, J. (2018). Derivatives and inverse of cascaded L+NL neural models. *PLoS 13(10):e0201326*.
- May, K. and Solomon, J. (2013). Four theorems on the psychometric function. *PLOS ONE*, 8(10):1–34.
- Pelli, D. G. (1991). Noise in the visual system may be early. pages 147–151. MIT Press.
- Pelli, D. G. and Farell, B. (1999). Why use noise? *Journal of the Optical Society of America A*, 16(3):647–653.
- Robson, J. G. (1966). Spatial and temporal contrast-sensitivity functions of the visual system. *Journal of the Optical Society of America*, 56(8):1141–1142.
- Schütt, H. and Wichmann, F. (2017). An image-computable psychophysical spatial vision model. *J. Vision*, 17(12):12.
- Sheikh, H. R. and Bovik, A. C. (2006). Image information and visual quality. *IEEE Trans. Img. Proc.*, 15(2):430–444.
- Simoncelli, E. P., Freeman, W. T., Adelson, E. H., and Heeger, D. J. (1992). Shiftable multi-scale transforms. *IEEE Trans Information Theory*, 38(2):587–607. Special Issue on Wavelets.
- Swets, J. A. (1961). Is There a Sensory Threshold? *Science (New York, N.Y.)*, 134(3473):168–177.

- Tanner, W. P. and Swets, J. A. (1954). A decision-making theory of visual detection. *Psychological Review*, 61(6):401–409.
- Wang, Z. and Simoncelli, E. P. (2008). Maximum differentiation (MAD) competition: A methodology for comparing computational models of perceptual quantities. *Journal of Vision*, 8(12):8–8.
- Watson, A. (1987). The cortex transform: Rapid computation of simulated neural images. *Computer Vision, Graphics and Image Processing*, 39:311–327.
- Watson, A. (1993). Visually optimal dct quantization matrices for individual images. In *[Proceedings] DCC '93: Data Compression Conference*, pages 178–187.
- Wichmann, F. (1999). *Some Aspects of Modelling Human Spatial Vision: Contrast Discrimination*. PhD thesis, Univ. of Oxford.
- Woods, J. and Stark, H. (2011). *Probability, Statistics, and Random Processes for Engineers*. Pearson Education.

## Appendix A: Derivation of Eq. 5 (general and particular cases)

**General case.** The theoretical distance in Eq. 4 can be written in terms of the stimulus and the different noise sources by using the Taylor approximation of the nonlinear behavior of the system, as already done in (Ahumada, 1987; Malo and Simoncelli, 2006), as follows:

$$S(x + \Delta x) \approx S(x) + \nabla S \cdot \Delta x \quad (11)$$

where  $\nabla S$  is the Jacobian of the model at  $x$ . This Taylor approximation is correct in the low-noise limit or if the nonlinearity of the system is moderate. Therefore, under this approximation,  $\Delta S = S(x + \Delta x) - S(x) = \nabla S \cdot \Delta x$ , and  $\Delta S^\top = \Delta x^\top \cdot \nabla S^\top$ , and the distance in Eq. 4 may be written as (Malo and Simoncelli, 2006):

$$D_{\text{th}}^2 = \Delta x^\top \cdot \nabla S^\top \cdot (\Sigma_{\mathcal{I}})^{-1} \cdot \nabla S \cdot \Delta x \quad (12)$$

Now, by definition, the covariance matrix of the *inner* noise  $\Sigma_{\mathcal{I}}$  is given by the expected value of the outer product of the noise:

$$\Sigma_{\mathcal{I}} = E [\mathbf{n}_{\mathcal{I}} \cdot \mathbf{n}_{\mathcal{I}}^\top] = E [(S(\mathbf{x} + \mathbf{n}_e + k\mathbf{n}_e) + k\mathbf{n}_l - S(\mathbf{x})) \cdot (S(\mathbf{x} + \mathbf{n}_e + k\mathbf{n}_e) + k\mathbf{n}_l - S(\mathbf{x}))^\top] \quad (13)$$

where, as stated in section 3.1, we included an unknown scale factor,  $k$ , in the early and the late noise. Using the Taylor expansion again, we have:

$$\begin{aligned} \Sigma_{\mathcal{I}} &= E [(\nabla S \cdot (\mathbf{n}_e + k\mathbf{n}_e) + k\mathbf{n}_l) \cdot ((\mathbf{n}_e + k\mathbf{n}_e)^\top \cdot \nabla S^\top + k\mathbf{n}_l^\top)] \\ &= k^2 E [\mathbf{n}_l \cdot \mathbf{n}_l^\top] + k^2 \nabla S \cdot E [\mathbf{n}_e \cdot \mathbf{n}_e^\top] \cdot \nabla S^\top + 2k E [\mathbf{n}_l \cdot \mathbf{n}_e^\top] \cdot \nabla S^\top + \\ &\quad + \nabla S \cdot E [\mathbf{n}_e \cdot \mathbf{n}_e^\top] \cdot \nabla S^\top + 2k \nabla S \cdot E [\mathbf{n}_e \cdot \mathbf{n}_e^\top] \cdot \nabla S^\top + 2k^2 E [\mathbf{n}_l \cdot \mathbf{n}_e^\top] \cdot \nabla S^\top \end{aligned} \quad (14)$$

where the expected value of crossed terms does not vanish in general because (1) the early noise may depend on the signal and hence it may depend on the external noise; and (2) the late noise may depend on the signal and hence may depend on the early and the external noise as well. In the above equation we can identify the terms of in Eq. 5:

$$\Sigma_{\mathcal{I}} = \underbrace{k^2 \Sigma_l}_{\text{late noise}} + \underbrace{k^2 \nabla S \Sigma_e \nabla S^\top}_{\text{early noise}} + \underbrace{2k^2 E[\mathbf{n}_l \mathbf{n}_e^\top] \nabla S^\top}_{\text{corr. late-early}} + \underbrace{\nabla S \Sigma_e \nabla S^\top}_{\text{external noise}} + \underbrace{2k \nabla S E[\mathbf{n}_e \mathbf{n}_e^\top] \nabla S^\top}_{\text{corr. early-external}} + \underbrace{2k E[\mathbf{n}_l \mathbf{n}_e^\top] \nabla S^\top}_{\text{corr. late-external}} \quad (15)$$

that represent how the covariance of the noise at the input is propagated through the network (Ahumada, 1987). The above equation contains the (general) covariance matrices of the late noise  $\Sigma_l$ , the early noise,  $\Sigma_e$ , and the external noise  $\Sigma_e$ , that may include arbitrary dependence with the signal. The next paragraph makes a particular choice for this variation.

**Particular case: Gaussian-Poisson noise.** If *early* and *late* noises are signal-dependent Gaussian-Poisson variables, their realizations are:

$$\begin{aligned}\mathbf{n}_e &= (\alpha_e I + \beta_e \mathbb{D}_{|\mathbf{x}|^{1/2}}) \cdot \mathbf{n}_{G1} \\ \mathbf{n}_l &= (\alpha_l I + \beta_l \mathbb{D}_{|S(\mathbf{x})|^{1/2}}) \cdot \mathbf{n}_{G2}\end{aligned}\quad (16)$$

where  $\mathbf{n}_{G1}$  and  $\mathbf{n}_{G2}$  denote realizations of unit covariance Gaussian noise in the input space and in the inner space (which have different dimension as there may be a different number of photoreceptors and cortical neurons), and  $\mathbb{D}_{(\cdot)}$  stands for a diagonal matrix with the elements of  $(\cdot)$  in the diagonal. The corresponding covariance matrices of the different noise sources can be written as:

$$\begin{aligned}\Sigma_e(\mathbf{x}) &= \alpha_e^2 I + \beta_e^2 \mathbb{D}_{|\mathbf{x}|} + 2\alpha_e \beta_e \mathbb{D}_{|\mathbf{x}|^{1/2}} \\ \Sigma_l(S(\mathbf{x})) &= \alpha_l^2 I + \beta_l^2 \mathbb{D}_{|S(\mathbf{x})|} + 2\alpha_l \beta_l \mathbb{D}_{|S(\mathbf{x})|^{1/2}}\end{aligned}\quad (17)$$

where  $\alpha_e^2$  is the variance of the Gaussian component of the early noise and  $\beta_e^2$  is the Fano factor of the Poisson component of the early noise, and equivalent concepts for the late noise.

In this work we assume that both the early and the late noise are pure Poisson sources, a usual assumption in neural systems (Brainard and Wandell, 2020; Dayan and Abbott, 2005), and hence our goal is determining the scale factors  $\beta_e$  and  $\beta_l$ .

## Appendix B: Optimization of correlation from Eq. 7

Instead of optimizing the noise through the metric using the mathematical expression for the distance shown in Eq. 5, which requires the derivative of the metric and, due to the inverse, this implies a dependence on  $(\Sigma_{\mathcal{I}})^{-2}$ , we suggest the optimization of the noise using a mathematical expression for the distance based on the difference in the noisy responses:

$$\begin{aligned}\mathbf{y}(\mathbf{x}) &= S(\mathbf{x}) + \mathbf{n}_{\mathcal{I}} \\ \mathbf{y}(\mathbf{x} + \Delta\mathbf{x}) &= S(\mathbf{x} + \Delta\mathbf{x}) + \mathbf{n}'_{\mathcal{I}} = \mathbf{y}(\mathbf{x}) + \Delta\mathbf{y}\end{aligned}\quad (18)$$

and take the average Euclidean distance between them, resulting in:

$$\begin{aligned}D_{\text{th}}^2 &= E[\Delta\mathbf{y}^\top \cdot \Delta\mathbf{y}] \\ &= E[|\Delta S + \mathbf{n}'_{\mathcal{I}} - \mathbf{n}_{\mathcal{I}}|^2]\end{aligned}\quad (19)$$

where  $\Delta S = S(\mathbf{x} + \Delta\mathbf{x}) - S(\mathbf{x})$  is the difference between the deterministic responses, and  $\mathbf{n}_{\mathcal{I}}$  and  $\mathbf{n}'_{\mathcal{I}}$  are different realizations of the *inner* noise at the points  $S(\mathbf{x})$  and  $S(\mathbf{x} + \Delta\mathbf{x})$ , respectively. Note that, as already said, Eq. 19 means that when judging the difference between two stimuli the brain compares two noisy responses,  $\mathbf{y}(\mathbf{x})$  and  $\mathbf{y}(\mathbf{x}) + \Delta\mathbf{y}$ , that is,  $S(\mathbf{x}) + \mathbf{n}_{\mathcal{I}}$  and  $S(\mathbf{x} + \Delta\mathbf{x}) + \mathbf{n}'_{\mathcal{I}}$ .

As stated above, our proposal for noise estimation explained in section 3.1 consisted of finding the noise parameters that maximize the correlation between the experimental  $D_{\text{exp}}$  and theoretical  $D_{\text{th}}$  distances. As shown in Eq. (S7.3) and (S7.5) in (Martinez et al., 2018), given  $n$  experimental conditions to measure  $n$  thresholds, the maximization of this correlation requires its derivative with regard to the parameters of the model, and reduces to computing  $\frac{\delta D_{\text{th}}^i}{\delta \theta}$ , where  $\theta$  are the noise parameters, and  $D_{\text{th}}^i$  is the distance for the  $i$ -th experimental condition, with  $i = 1, \dots, n$ . According to Eq. (S7.6) in (Martinez et al., 2018), these derivatives can be written as:

$$\frac{\delta D_{\text{th}}^i}{\delta \theta} = \frac{1}{D_{\text{th}}^i} \cdot (\mathbf{y}(x^i + \Delta x^i) - \mathbf{y}(x^i))^\top \cdot \left[ \frac{\delta \mathbf{y}(x^i + \Delta x^i)}{\delta \theta} - \frac{\delta \mathbf{y}(x^i)}{\delta \theta} \right]\quad (20)$$

To compute the derivatives  $\frac{\delta \mathbf{y}(\cdot)}{\delta \theta}$  we can apply the Taylor approximation to Eq. 1 to get:

$$\mathbf{y}(\mathbf{x}) = S(\mathbf{x} + \mathbf{n}_\varepsilon + \mathbf{n}_e) + \mathbf{n}_l \approx S(\mathbf{x}) + \nabla S \cdot \mathbf{n}^\varepsilon + \nabla S \cdot \mathbf{n}_e + \mathbf{n}_l\quad (21)$$

And now, for the case in which *early* and *late* noises are signal-dependent Gaussian-Poisson variables, plugging Eq. 16 into Eq. 21 we obtain:

$$\mathbf{y}(\mathbf{x}) = S(\mathbf{x}) + \nabla S \cdot \mathbf{n}^\varepsilon + \nabla S \cdot (\alpha_e I + \beta_e \mathbb{D}_{|\mathbf{x}|^{1/2}}) \cdot \mathbf{n}_{G1} + (\alpha_l I + \beta_l \mathbb{D}_{|S(\mathbf{x} + \mathbf{n}_\varepsilon + \mathbf{n}_e)|^{1/2}}) \cdot \mathbf{n}_{G2} \quad (22)$$

Applying again the Taylor approximation to the term  $|S(\mathbf{x} + \mathbf{n}_\varepsilon + \mathbf{n}_e)|^{1/2}$  we finally get:

$$\mathbf{y}(\mathbf{x}) = S + \nabla S \cdot \mathbf{n}^\varepsilon + \nabla S \cdot (\alpha_e I + \beta_e \mathbb{D}_{|\mathbf{x}|^{1/2}}) \cdot \mathbf{n}_{G1} + \left( \alpha_l I + \beta_l \mathbb{D}_{|S|^{1/2} + \frac{1}{2}|S|^{-1/2} \cdot \text{sign}(S) \cdot \nabla S \cdot (\mathbf{n}_\varepsilon + \mathbf{n}_e)} \right) \cdot \mathbf{n}_{G2} \quad (23)$$

where for readability the function  $S(\mathbf{x})$  has been named  $S$ , and the function  $\text{sign}(\cdot)$  applies the sign of  $(\cdot)$ .

With this result for  $\mathbf{y}(\mathbf{x})$  it is possible to obtain the derivatives wrt the *early*  $(\alpha_e, \beta_e)$  and *late*  $(\alpha_l, \beta_l)$  noise parameters that are needed to maximize the correlation between the experimental  $D_{\text{exp}}$  and theoretical  $D_{\text{th}}$  distances:

$$\begin{aligned} \frac{\delta \mathbf{y}(\mathbf{x})}{\delta \alpha_e} &= \nabla S \cdot I \cdot \mathbf{n}_{G1} + \left( \beta_l \mathbb{D}_{\frac{1}{2}|S|^{-1/2} \cdot \text{sign}(S) \cdot \nabla S \cdot \mathbf{n}_{G1}} \right) \cdot \mathbf{n}_{G2} \\ \frac{\delta \mathbf{y}(\mathbf{x})}{\delta \beta_e} &= \nabla S \cdot \mathbb{D}_{|\mathbf{x}|^{1/2}} \cdot \mathbf{n}_{G1} + \left( \beta_l \mathbb{D}_{\frac{1}{2}|S|^{-1/2} \cdot \text{sign}(S) \cdot \nabla S \cdot \mathbb{D}_{|\mathbf{x}|^{-1/2}} \cdot \mathbf{n}_{G1}} \right) \cdot \mathbf{n}_{G2} \\ \frac{\delta \mathbf{y}(\mathbf{x})}{\delta \alpha_l} &= \mathbf{n}_{G2} \\ \frac{\delta \mathbf{y}(\mathbf{x})}{\delta \beta_l} &= \left( \mathbb{D}_{|S|^{1/2} + \frac{1}{2}|S|^{-1/2} \cdot \text{sign}(S) \cdot \nabla S \cdot (\alpha_e I + \beta_e \mathbb{D}_{|\mathbf{x}|^{1/2}})} \cdot \mathbf{n}_{G1} \right) \cdot \mathbf{n}_{G2} \end{aligned} \quad (24)$$

As can be seen from these last equations, in this non-parametric case the derivatives wrt the *early* and *late* noise parameters do not involve matrix inversion, and hence they are easy to compute. This allows a practical optimization of the noise parameters to maximize the correlation between the experimental and theoretical distances, no matter the complexity of the noise, whenever  $\nabla S$  is easy to compute.

## Appendix C: Equivalence of parametric and non-parametric distances

In this appendix we show that the considered distances, Eq. 5 and Eq. 7, are equally valid to get the corresponding estimation of the noise. First we show that the distances have an interesting anisotropic behavior depending on the noise: perceptual distance is markedly different for distortions in different directions  $\Delta \mathbf{x}$ . The noise-dependent anisotropy is obvious in Eq. 5 because the metric depends on the covariance of the noise, but this is less obvious in the non-parametric Eq. 7.

The first part of this Appendix analytically shows that the non-parametric distance displays this anisotropy. Afterwards, we numerically show that the distance computed in both ways can be linearly related. As a result, since correlation is independent of a linear transformation applied to one of the axis, both definitions of  $D_{\text{th}}$  are equivalent for our purposes.

**Analytical part: non-parametric distance is anisotropic.** The general expression for the average Euclidean distance in the non-parametric case, Eq. 19,  $D_{\text{th}}^2 = E \left[ |\Delta S + \mathbf{n}'_{\mathcal{I}} - \mathbf{n}_{\mathcal{I}}|^2 \right]$ , can be written as:

$$D_{\text{th}}^2 = E \left[ (\Delta S + (\mathbf{n}'_{\mathcal{I}} - \mathbf{n}_{\mathcal{I}}))^{\top} \cdot (\Delta S + (\mathbf{n}'_{\mathcal{I}} - \mathbf{n}_{\mathcal{I}})) \right] \quad (25)$$

which can be expanded as follows:

$$\begin{aligned} D_{\text{th}}^2 &= E \left[ \Delta S^{\top} \cdot \Delta S + \Delta S^{\top} \cdot (\mathbf{n}'_{\mathcal{I}} - \mathbf{n}_{\mathcal{I}}) + (\mathbf{n}'_{\mathcal{I}} - \mathbf{n}_{\mathcal{I}})^{\top} \cdot \Delta S + (\mathbf{n}'_{\mathcal{I}} - \mathbf{n}_{\mathcal{I}})^{\top} \cdot (\mathbf{n}'_{\mathcal{I}} - \mathbf{n}_{\mathcal{I}}) \right] \\ &= \Delta S^{\top} \cdot \Delta S + 2 E \left[ \Delta S^{\top} \cdot (\mathbf{n}'_{\mathcal{I}} - \mathbf{n}_{\mathcal{I}}) \right] + E \left[ \mathbf{n}'_{\mathcal{I}}^{\top} \cdot \mathbf{n}'_{\mathcal{I}} \right] - 2 E \left[ \mathbf{n}'_{\mathcal{I}}^{\top} \cdot \mathbf{n}_{\mathcal{I}} \right] + E \left[ \mathbf{n}_{\mathcal{I}}^{\top} \cdot \mathbf{n}_{\mathcal{I}} \right] \\ &= |\Delta S|^2 + |\mathbf{n}_{\mathcal{I}}|^2 + |\mathbf{n}'_{\mathcal{I}}|^2 - 2 E \left[ \mathbf{n}'_{\mathcal{I}}^{\top} \cdot \mathbf{n}_{\mathcal{I}} \right] + 2 E \left[ \Delta S^{\top} \cdot (\mathbf{n}'_{\mathcal{I}} - \mathbf{n}_{\mathcal{I}}) \right] \end{aligned} \quad (26)$$

where the last term vanishes because it compares a deterministic component and a random component. When  $\Delta S = 0$ ,  $\mathbf{n}'_{\mathcal{I}} = \mathbf{n}_{\mathcal{I}}$ , and then,  $2 E \left[ \mathbf{n}'_{\mathcal{I}}^{\top} \cdot \mathbf{n}_{\mathcal{I}} \right] = 2 |\mathbf{n}_{\mathcal{I}}|^2$ , so  $D_{\text{th}}^2 = 0$ . When  $\Delta S \neq 0$ , as  $\mathbf{n}_{\mathcal{I}}$  and  $\mathbf{n}'_{\mathcal{I}}$  are decorrelated,  $E \left[ \mathbf{n}'_{\mathcal{I}}^{\top} \cdot \mathbf{n}_{\mathcal{I}} \right] = 0$ , so we get:

$$D_{\text{th}}^2 = |\Delta S|^2 + |\mathbf{n}_{\mathcal{I}}|^2 + |\mathbf{n}'_{\mathcal{I}}|^2 \quad (27)$$

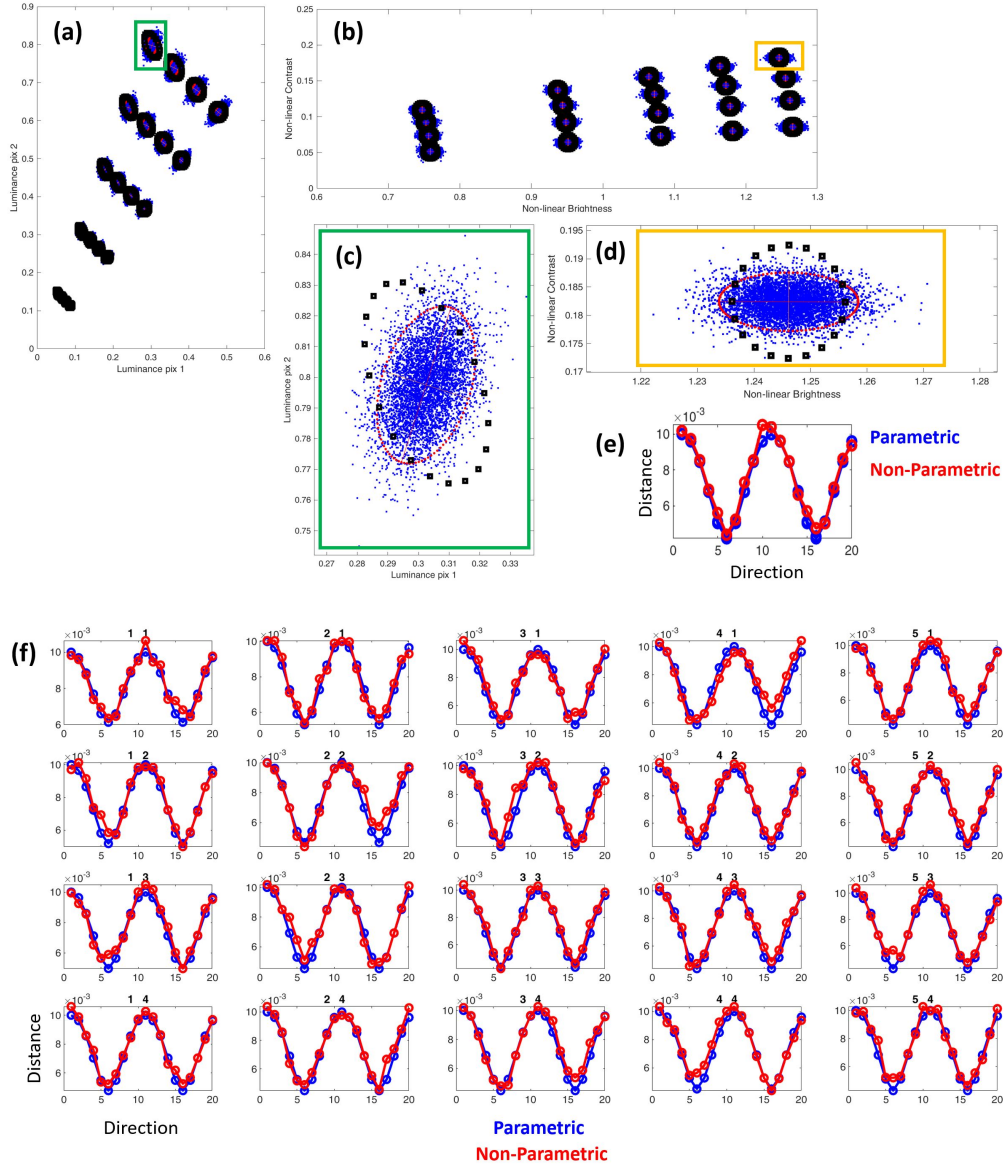


Figure 8: **Equivalence between parametric and non-parametric distances.** Plots (a) and (b) show the  $4 \times 5$  locations (4 contrasts times 5 luminances) considered in the space of 2-pixel images and in the inner representation of the illustrative model introduced in Section 2.3. The noisy images and responses are represented by the random samples in blue. Plots (c) and (d) zoom the highlighted rectangles in green and orange. In each location in the internal representation we computed distances from the central point in the directions indicated by the black squares. The plot (e) represents the distances from the central point in plot (d) in the different directions computed through the parametric and non-parametric methods, Eqs. 5 and 7, in blue and red respectively. The plots in panel (f) show the same result at the other considered points all over the image space.

Note that, in this expression,  $|\Delta S|$  and  $|n_{\mathcal{I}}|$  are constants for a given  $\mathbf{x}$ . However, in general, the energy  $|n'_{\mathcal{I}}|^2$  depends on  $\Delta \mathbf{x}$  (or  $\Delta S$ ). This dependence is what generates the anisotropic behavior of the distance. For instance, if the *inner* noise has a Poisson component, the direction of  $\Delta S$  matters: increasing the response in a certain direction may increase the energy, while going in the opposite direction (reducing the response) may reduce the energy of the noise.



**Numerical illustration: non-parametric and parametric distances are linearly related.** In this section we use the simplified vision model introduced in Section 2.3 (on 2-pixel images) to illustrate explicitly how the non-parametric distance of Eq. 7 follows the trends of the parametric metric in Eq. 5. Using the model implemented here<sup>6</sup> we considered  $4 \times 5$  locations (4 contrasts times 5 luminances) in the space of 2-pixel images, and we generated 5000 noisy responses for each of these images. See the noisy samples and responses in Fig. 8. Then, we considered 20 points at constant Euclidean distance from each average response in equidistant directions along the Euclidean sphere, e.g. the black squares in the zoom Fig. 8.d. These points are convenient to point out the anisotropy of the measures and their eventual equivalence.

The metric defined by the noisy samples implies that the locus of equidistant points from the center is the ellipsoid highlighted in red. As a result, the perceptual metric is anisotropic: starting from the vertical direction in Fig. 8.d, the distance is maximum and it goes down and up in a periodic way, as given by the blue line in plot 8.e, computed according to the parametric distance. The distance of each black square was also computed from the expected value in Eq. 7 leading to the red curve in plot 8.e. The plots in the panel (f) show that the equivalence between the two measures holds all over the image space with the same linear relation between the parametric and non-parametric measures. All the curves in red were obtained from the non-parametric distances and the same linear relation with the parametric distance.

In summary, the (simpler to compute) non-parametric distance based on the average over the noisy samples is equivalent, i.e. leads to the same correlation, as the parametric distance which requires the inversion of huge matrices in the optimization.

## Appendix D: Noise from thresholds for individual observers

The surfaces in Figure 9 show the correlation between the threshold-based experimental distances and the theoretical distances based on pure Poisson early and late noise for each individual observer. In this case the data of each observer is considered separately, so we obtain different optima (highlighted in red) for each observer. The scatter plots on top show the predictions with better linear correlation.

In this threshold-only method separation of data per observer does not improve the optimization problem: similarly to Fig. 2 the correlation surfaces display large plateaus of almost constant values thus indicating uncertainty in the optima. Moreover, observers display quite different results. In particular observer GBH seems to drive the global result in Fig. 2 because the data from observer CMB displays small correlation anyway and has small impact in the global correlation.

This uncertainty and disparity is in contrast with the narrow minima and consistency between observers found in the method that considers all the data in the psychometric functions (Fig. 4). This suggests that the consideration of the full psychometric functions properly constrain the problem towards more accurate and consistent solutions.

## Appendix E: Physiological estimates of early noise using ISETBIO

Here we described how we used ISETBIO (Brainard and Wandell, 2020) to get a reasonable physiological estimation of retinal noise, which, in principle, would be the physiological correlate of our psychophysical early noise estimate. Nevertheless, the results clarify why the comparison is not straightforward and why it is sensible to have one order of magnitude less noise in a psychophysical model.

ISETBIO (Brainard and Wandell, 2020), allows the definition of a stimulus in physical units, e.g. an achromatic stimulus (flat spectral radiance) of certain luminance in  $cd/m^2$ , and subtending certain degrees in the visual field. The software incorporates accurate models of the human optics and of retina photoreceptors, so it computes both the blurred image at the retina and models the isomerization process so that the retinal image is transformed in noisy photocurrents at the L, M and S sensors. This happens dynamically and incorporates fixation and microsaccade motion.

<sup>6</sup><http://isp.uv.es/code/visioncolor/noise.html>

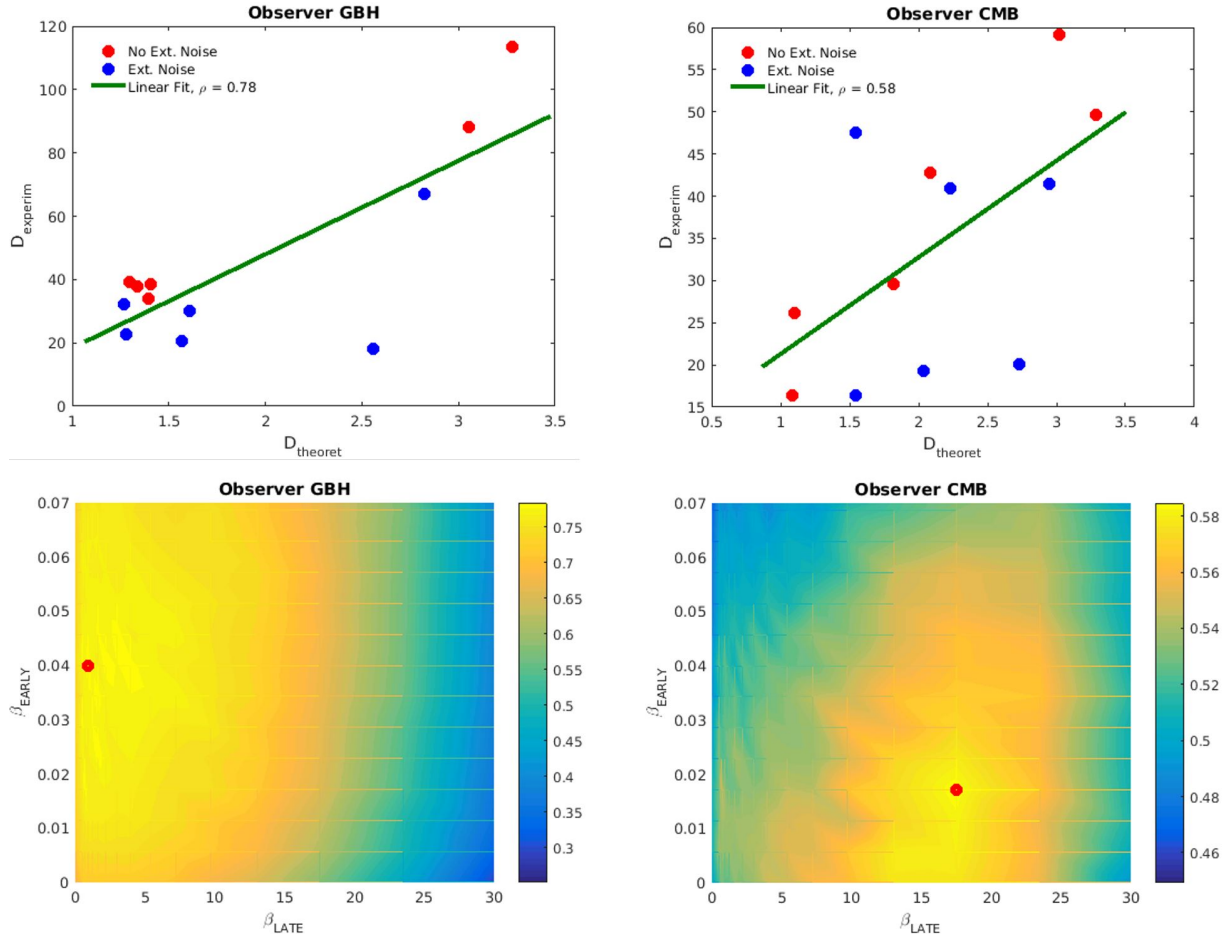


Figure 9: **Early and late noise parameters from threshold data for each individual observer.** The top plots represent the best (maximum correlation) linear fits between the theoretical distance (that depends on the noise sources) and the experimental distance (based on the thresholds) for the considered observers. The surfaces at the bottom display the correlation between the theoretical distance and the experimental distance depending on the noise parameters. The optimal noise parameters, here highlighted in red, are those that maximize the correlation for each observer ( $\beta_e = 0.04$ ,  $\beta_l = 0.91$ ) for GBH and ( $\beta_e = 0.02$ ,  $\beta_l = 17.5$ ) for CMB.

One can use this accurate model to estimate the noise added to the input in  $cd/m^2$  units by doing two things: (1) modeling the relation between input luminance and brightness expressed in terms of cone photocurrents, and (2) computing the noise in the brightness domain and transforming it back to luminance using the inverse of the luminance-brightness relation. In particular, we used the demo `t_dynamicStimulusToPhotocurrent.m` with default parameters. We just modified the function to have access to intermediate results or switch on/off the eye motion model when necessary, but we did not change the default choices.

The estimation of the luminance-brightness relation is easy to do assuming that the brightness perception is driven by the sum of the responses of the L and M cones, as is usual in color vision models (Fairchild, 2013). By doing so, one can build a series of stimuli of different luminance, see the top row of Fig. 10, and register the L+M responses in  $pA$ .

In order to compare the spatial description of the stimuli and the photoreceptor mosaic we spatially interpolated the L and M mosaics using linear interpolation (i.e. we introduced minimal spatial blur). In particular, we didn't assume the wider spatial summation happening down stream in retinal ganglion cells or LGN cells.

We used Gabors of 2 cpd with different average luminance and fixed contrast and put them through the model to empirically derive

a luminance-photocurrent function. The responses integrated over short periods of time (e.g. 200 msec) display a substantial amount of noise but the average value of L+M in  $pA$  can be used to derive a simple input-output curve that can be interpreted as a luminance-brightness response. The nonlinear plots at the right of Fig. 10 display such curves (the top one in  $pA$  and the bottom one re-scaled to have values in the range of the input luminance). We fitted a conventional exponential function to transform the input luminance into this *brightness*: see the parameters of the fit in the bottom-right figure. This function can be inverted in order to transform photocurrents into luminance values.

This inverse is the one that allows us to represent the noisy responses obtained using short exposure times (200 msec) in a luminance scale (as for instance the second row of responses to the stimuli shown in the first row).

We explicitly checked that the ocular motion has no effect in this estimation. Consistently with the reports in (?), the speed induced by the ocular motion in ISETBIO is about 0.1 deg/sec, which, in 200 msec just implies a spatial displacement of 0.02 degrees, which is small to induce a major luminance change in the 2cpd Gabors used in our experiment. Therefore the luminance-photocurrent curves do not change if we switch off the ocular motion in the model.

We estimated the noise in the brightness domain by subtracting this noisy L+M signal integrated over a short period of time (200 msec) from the equivalent signal averaged over a large exposure time to "artificially" remove all the noise in the response. In this second long-exposure-time case (where we integrated over 8 seconds) we switch off the ocular motion in the model so that the noise removal does not come from changes in the spatial structure of the input. The temporally-denoised responses in luminance units can be seen in the third row of Fig. 10. The subtraction of the clean response (3rd row) from the noisy responses (2nd row) leads to the noise realizations shown in the 4th row of the figure. In this row that displays the physiological noise for different input luminance it is obvious that the variance of this noise increases with the input luminance.

Measuring the standard deviation of the noise in this series of realizations in the 4th row one can obtain the result shown in Fig. 7: according to ISETBIO the standard deviation of the noise at the retina depends on the luminance  $L$  as:  $\sigma_{\text{retina}} \approx 0.33 * L^{0.57}$  ( $cd/m^2$ ).

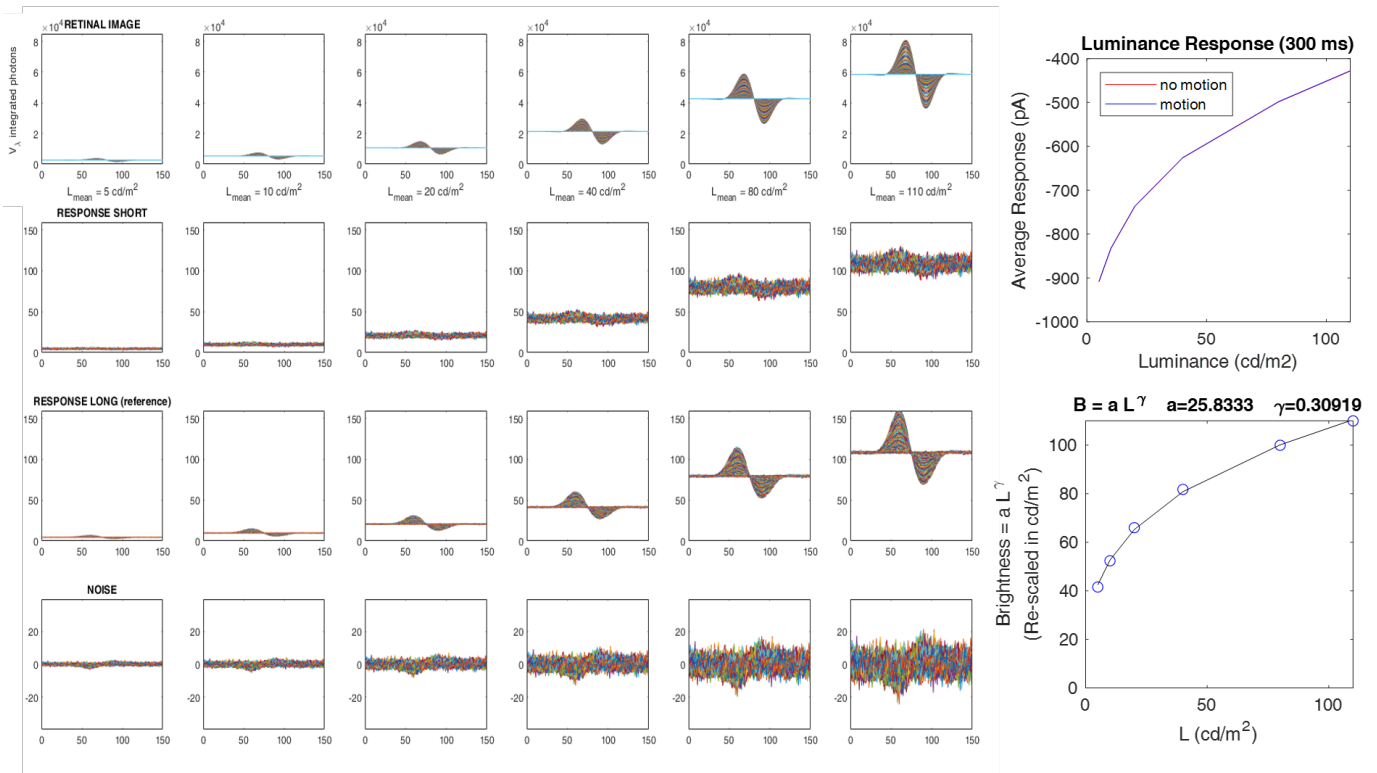


Figure 10: **Procedure to estimate retinal noise in  $cd/m^2$  using ISETBIO.** Top row represents a series of achromatic Gabors of 2cpd of fixed contrast with controlled luminance. Top-right plot displays the nonlinear relation between input luminance and L+M photocurrents in  $pA$  (with 200 msec exposure time). Bottom-right plot displays the same relation where the vertical axis has been re-scaled to have values in the luminance range. The plot also displays the parameters of a exponential luminance-brightness fit. The responses of the ISETBIO retina corresponding to the stimuli in the 1st row, using either a short exposure time (hence noisy) and averaged over a long exposure time (hence de-noised) are shown in the 2nd and 3rd rows respectively. The luminance-brightness fit has been used to express the responses of the 2nd and 3rd rows (given in  $pA$  by ISETBIO) in luminance units ( $cd/m^2$ ). The subtraction of the 2nd and 3rd rows leads to the noises estimated in the 4th row.